Journal of Multiscale Neuroscience

Original Research

Spatial interactions impact on Ca-driven synaptic plasticity: An ionic cable theory perspective

Nicolangelo Iannella[1,*], Roman R. Poznanski[2]
[1]The Faculty of Mathematics and Natural Sciences, University of Oslo, Oslo 0316 Norway
[2]Integrative Neuroscience Initiative, Melbourne Australia 3145

*Corresponding author: n.l.iannella@ibv.uio.no
DOI:https://doi.org/10.56280/1631287433

Received: 26 November 2023 Accepted: 15 May 2024 Online published 31 May 2024

Abstract

We extend our previous paper on deriving an approximate analytical solution to a nonlinear cable equation by including other ion channels known to exist in neurons and reaction-diffusion-based calcium dynamics that lead to a system of nonlinear cable equations. Here, excitable dendrites possess clusters of voltage-activated ion channels that are discretely distributed as point sources or hotspots of transmembrane current along a continuous cable structure of fixed length. Single and/or trains of action potentials along with spatially distributed synaptic inputs drive the depolarisation and activate sparsely distributed voltage-dependent calcium channels leading to calcium influx and diffusion in the cable. Here, time-dependent analytical solutions were obtained through the application of a perturbation expansion of the non-dimensional voltage (Φ) and non-dimensional calcium (Φ^{Ca}) and then solving the resulting set of integral equations. We use this framework to gain insights to calcium-driven synaptic plasticity in dendrites. Previous studies have traditionally focused on the local impact of calcium on whether the strength of the synapse is increased (potentiated) or decreased (depressed). Only recently, studies focusing on heterosynaptic plasticity have been gaining popularity and here we ask the question of how a local plasticity rule is influenced by the spatially and temporally distributed synaptic inputs. Specifically, we focus on how the resulting spike-timing-dependent plasticity (STDP) window is influenced by synaptic inputs and calcium influx at nearby sites to assess the nature of the resulting distance-dependent heterosynaptic interaction on STDP at the synapse of interest.

Keywords: Ion channels, Spike trains, Sparsely excitable dendrites, Integrative modelling, Ionic cable equation, Green's functions, calcium-based synaptic plasticity, Spike timing-dependent plasticity (STDP).

1. Introduction

Many papers, both experimental and theoretical have focused on how interconnected populations of neurons adapt their connectivity and functional properties, in response to neural activity caused by some external stimulus. At the cellular level, experimental observation of this activity drives changes in both the pattern of connectivity and the strength of synapses between neurons. High-frequency activity or pairing low-frequency stimulation with depolarisation at the postsynaptic site has typically demonstrated the strengthening of the synaptic weight, an effect commonly known as Long-Term Potentiation (LTP) (Bliss & Lomo, 1973; Dudek & Bear, 1992 1993; Levy & Steward, 1979; Stent, 1973) while low-frequency stimulation alone leads to the weakening of the synapse called Long-Term Depression (LTD) (Abraham & Goddard, 1983; Barrionuevo et al., 1980; Fujii et al., 1991; Levy & Steward, 1979; Staubli & Lynch, 1990). These studies have also illustrated the additional properties of associativity and cooperativity between synapses involved in the induction of LTP or LTD. Moreover, such studies have shown distinct types of LTP and LTD are expressed in different cellular domains (Frey & Morris, 1997; Malenka et al., 1989; Mulkey et al., 1993).

Nevertheless, experiments have additionally illustrated that the property of temporal specificity also contributes to the direction of synaptic change. This spike-timing-dependent plasticity illustrated that the temporal order and precise timing of presynaptic and postsynaptic activities govern the change in synaptic strength, whose functional profile is described by an asymmetric temporal window where synaptic potentiation occurs when presynaptic activity precedes postsynaptic spike generation; and synaptic weakening occurs when the temporal order of such events is reversed (Bi & Poo, 1998; Debanne et al., 1994 1998 1995; Markram et al., 1997; Zhang et al., 1998).

For over three decades studies have demonstrated that the type of stimulation is not the only factor that is involved neural learning, but there are contributions from intracellular processes; the most notable being the role and contribution of calcium and other molecules (De Schutter & Smolen, 1998; Frey & Morris, 1997 1998; Kelleher et al., 2004; Reymann & Frey, 2007; Sajikumar & Frey, 2004*ab*; Sajikumar et al., 2007 2004; Smolen, 2007). Recent studies have increasingly turned their attention to understanding the molecular processes of how synapses change, both structurally and functionally, and thus require a comprehensive understanding of the underlying molecular signalling network and the corresponding interactions between various molecules, which remains elusive. Nonetheless, numerous experiments have underscored the pivotal role of fluctuations in cellular calcium levels in facilitating plastic changes in synapses. We that the nonlinear voltage dependency of the N-Methyl-D-Aspartate (NMDA) receptor dictates that modest activation induces Long-Term Depression (LTD), whereas robust activation triggers Long-Term Potentiation (LTP) (Dudek & Bear, 1992 1993; Kirkwood et al., 1996; Malenka et al., 1988). Moreover, the initiation of either LTD or LTP consistently corresponds to subsequent alterations in intracellular calcium levels within the synapse, typically through calcium influx via NMDA receptor activation. Nevertheless, NMDA receptor activation represents just one avenue through which calcium influx into the synapse can occur; activation of high-voltage-activated L-type and low-voltage-activated T-type calcium channels or calcium release from internal stores, such as the endoplasmic recticulum (ER) can also precipitate altering in intracellular calcium levels.

One topic that has gained increasing attention is the role and induction of heterosynaptic plasticity within dendrites, where the induction of synaptic plasticity caused by pre-synaptic and post-synaptic activity at one position causes plasticity changes at different nearby locations (Chater & Goda, 2021; Chistiakova & Volgushev, 2009; Moldwin et al., 2023; Pozo & Goda, 2010; Tong et al., 2021). This points to the question that deserves further investigation of the role that the spatial spread of internal calcium has on the plasticity of synapses and specifically, the interplay between neuronal morphology on the spread of activity within dendrites and how this affects calcium concentration and the expression of synaptic plasticity. One related example is the distance-dependent broadening of the LTD component of the STDP learning window along the apical dendrite of a layer 2/3 pyramidal cell presented by (Froemke et al., 2005) and this heterogeneity points to location-dependent modifications that affect local activity and plastic change of synapse, a view supported by the existence of a cooperative switch in the sign of plasticity in distal dendrites of neocortical pyramidal cells (Sjöström & Häusser, 2006). The multifacet aspects towards understanding the heterosynaptic nature of synaptic plasticity within dendrites naturally lead one to ask about the contribution of distance-dependent spatial interactions resulting from spatially and temporally distributed inputs and the corresponding calcium influx on the associated learning window at the synaptic location of interest.

In tandem with conducting experiments, the cultivation of theoretical frameworks can enhance comprehension regarding the mechanisms and consequences of different types of plasticity, and the central role of calcium (and other important macromolecules). These theoretical tools facilitate the formulation of predictions and valuable insights into the dynamic interaction between activity and cellular calcium levels, during synaptic plasticity induction. To meet such a challenge, ionic cable theory has been developed which takes into account the physically discrete distribution and voltage-dependent

nature of ion channels throughout the neuron's membrane and permits analytical solutions to be obtained (Poznanski, 2001 2004; Poznanski & Bell, 2000*ab*). Significantly, this framework has been extended to include the reaction and diffusion of calcium in dendritic cables and was shown to reproduce the distance-dependent broadening of the LTD portion of the STDP learning window (Iannella & Tanaka, 2006 2007; Iannella et al., 2014), highlighting the importance to consider the influence of neuronal morphology on plasticity outcomes.

In this paper, we investigate one of many aspects associated with heterosynaptic plasticity, namely the impact of how spatial interactions between synaptic inputs influence the level of intracellular calcium and the expression of plasticity. Significantly, our study predicts that the nature of synaptic summation introduces a distance-dependent spatiotemporal influence on the expression of plasticity. We illustrate this effect through a simple simulation paradigm that can be easily adopted in experiments where we supplement the STDP protocol with an additional short train of input spikes at various spatial locations close to the site of interest and whose timing is delayed concerning this site, thus providing a picture of the nontrivial nature of heterosynaptic interactions and their associated spatiotemporal effects.

2. Methods

We use Shouval's widely accepted calcium-dependent plasticity (CaDP) model (Shouval et al., 2002) to investigate the distance-dependence and temporal influence that short trains of input spikes have on the expression of calcium-dependent synaptic plasticity at a given site of interest to help uncover associated spatiotemporal effects.

In the original model proposed by Shouval et al. (2002), plasticity occurs through a singular point of association, hinging on the interplay between glutamatergic NMDA receptor activation and (strong) depolarisation of a dendrite's postsynaptic membrane. Here, NMDA serves as a coincidence detector between pre- and postsynaptic activities. The model explicitly incorporates the calcium control hypothesis, positing that moderate calcium levels above a baseline induce long-term depression (LTD), whereas elevated calcium levels prompt long-term potentiation (LTP). Additionally, this study refrains from introducing location-specific variations in the parameters of the plasticity rule to prevent potential confounding effects. Shouval's original model for CaDP is given by the following set of equations,

$$\begin{aligned} \frac{dW_j}{dt} &= \eta\left([\mathrm{Ca}^{2+}]_j\right)\left(\Omega\left([\mathrm{Ca}^{2+}]_j\right) - W_j\right), \\ \Omega(x) &= \sigma(x-a_2,b_2) - A\sigma(x-a_1,b_1), \\ \eta(x) &= \frac{p_2 + x^{p_3}}{p_1 + p_4(p_2 + x^{p_3})}, \\ \sigma(x,a) &= \frac{e^{ax}}{1+e^{ax}}, \end{aligned} \tag{1}$$

where W_j denotes the strength of synapse j, $[\mathrm{Ca}^{2+}]_j$ is the peak calcium concentration at that synapse, $\eta\left(\left[\mathrm{Ca}^{2+}\right]_j\right)$ is a calcium-dependent learning rate, and $\Omega\left(\left[\mathrm{Ca}^{2+}\right]_j\right)$ determines the sign of synaptic change as a function of calcium concentration $\left[\mathrm{Ca}^{2+}\right]_j$ in synapse j. The calcium dependent functions $\Omega(x)$ and $\eta(x)$ are illustrated in **Fig 1A and Fig 1B**, respectively. The weight change to a single presynaptic and postsynaptic pairing is proportional to

$$\Delta W_j \propto \eta\left([\mathrm{Ca}^{2+}]_j\right)\Omega\left([\mathrm{Ca}^{2+}]_j\right). \tag{2}$$

We start by considering a section of dendrite described by our ionic cable framework, as a continuous cable where voltage is denoted by $V(x,t)$ (mV) and calcium concentration by $[Ca](x,t)$ (μM), endowed with various voltage-dependent ion channels and calcium dynamics. Our set of ion channels is described using the Hodgkin-Huxley formalism, comprising of sodium, the delayed rectifier and transient potassium, Low voltage-activated (LVA) and high voltage-activated (HVA) calcium channels distributed along the cable at discrete locations forming hotspots that contain clusters of channels acting as point current sources. Furthermore, we also consider hotspots of α-amino-3-hydroxy-5-methyl-4-isoxazolepropionic acid (AMPA), gamma-aminobutyric acid (GABA), and N-methyl-d-aspartate (NMDA) receptors, that represent the post-synaptic side of our synapse(s). Our model is mathematically described by the following system of reaction-diffusion equations

(A)

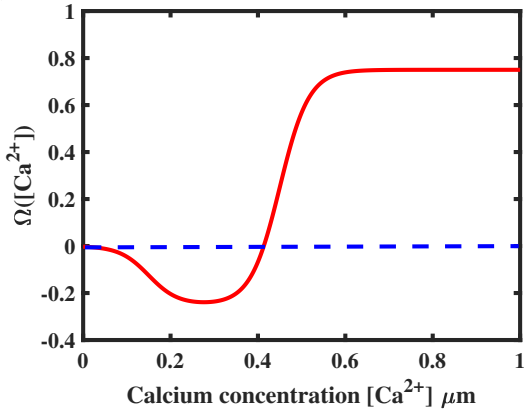

(B)

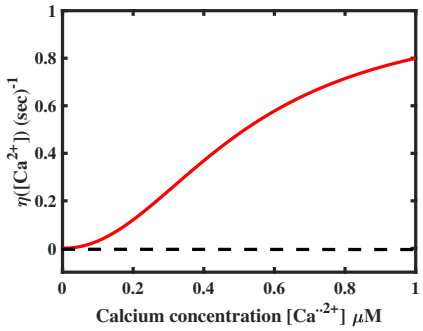

Figure 1: **(A):** The calcium-dependent function $\Omega([\mathrm{Ca}^{2+}]_j)$ implements the calcium control hypothesis, when $[\mathrm{Ca}^{2+}] < \theta_d$ no change in the synaptic weight occurs, for $\theta_d < [\mathrm{Ca}^{2+}] < \theta_p$ synaptic depression (LTD) occurs, and for $[\mathrm{Ca}^{2+}] > \theta_p$ synaptic weights are increased (LTP) (parameters used were $A = 0.25$, $a_1 = 0.45$, $a_2 = 30$, $a_3 = 0.65$, $a_4 = 30$. **B:** Calcium dependent learning rate η (adapted from Shouval et al. (2002)). Parameters were $p_1 = 0.25$, $p_2 = 1/10000$, $p_3 = 2.1$, $p_4 = 1$.

given by,

$$
\begin{aligned}
C_m \frac{\partial V}{\partial t} &= \frac{d}{4\rho_i}\frac{\partial^2 V}{\partial x^2} + g_\ell(V_\ell - V) \\
&+ \sum_{\mu=1}^{k}\sum_{i=1}^{N_\mu} I^{\mu}_{ion}(x,t;V;Ca)\delta(x - x^{\mu}_i) \\
&+ \sum_{i=1}^{N_{\mathrm{AMPA}}} I^{\mathrm{AMPA}}(x,t;V)\delta(x - x^{\mathrm{AMPA}}_i) \\
&+ \sum_{i=1}^{N_{\mathrm{NMDA}}} I^{\mathrm{NMDA}}(x,t;V;Ca)\delta(x - x^{\mathrm{NMDA}}_i) \\
&+ \sum_{i=1}^{N_{\mathrm{GABA}}} I^{\mathrm{GABA}}(x,t;V)\delta(x - x^{\mathrm{GABA}}_i) + \bar{I}_A(x,t)
\end{aligned}
$$

$$
\begin{aligned}
\frac{\partial [Ca]_i}{\partial t} &= D_{Ca}\frac{\partial^2 [Ca]_i}{\partial x^2} + b_M[M] - f_M[Ca]_i\mathcal{B}^T_M \\
&+ f_M[Ca]_i[M] - \frac{4P_m}{d}K_p\frac{[Ca]_i}{[Ca]_i + K_p} \\
&+ \sum_{\nu=1}^{s}\sum_{i=1}^{N_\nu}\frac{2\mathcal{I}^{\nu}_{Ca}(x,t;V;Ca)}{\mathcal{F}d}\delta(x - x^{\nu}_i) \\
&+ \sum_{i=1}^{N_{\mathrm{NMDA}}}\frac{2\mathcal{I}^{\mathrm{NMDA}}_{\mathrm{Ca}}(x,t;V;Ca)}{\mathcal{F}d}\delta(x - x^{\mathrm{NMDA}}_i) \\
\frac{\partial [M]}{\partial t} &= D_M\frac{\partial^2 [M]}{\partial x^2} - b_M[M] \\
&+ f_M[Ca]_i\mathcal{B}^T_M - f_M[Ca]_i[M], \qquad (3)
\end{aligned}
$$

where C_m is the membrane capacitance per unit area (F/cm^2), d is the diameter of the finite cable under consideration, ρ_i is the internal cytoplasmic resistivity (Ωcm), g_ℓ is the leak conductance with units (S/cm^2) and V_ℓ is the leak reversal potential (mV). I^{μ}_{ion} represents the ion current density per unit length (mA/cm) (which can either be voltage-dependent, calcium-dependent or both) for a single type of channel, denoted by μ. $\bar{I}_A(x,t)$ is an applied current density per unit area (mA/cm^2), and δ is the Dirac delta function (cm^{-1}), where N_μ and x^{μ}_i, are the numbers and positions of hotspots for each channel μ, respectively.

In addition, $[Ca]_i$ and $[M]$ are the respective internal calcium and buffer concentrations in (μM) at position x and time t and $\mathcal{B}^T_M$ denotes the total concentration of buffer $\mathcal{B}_M$, and the diffusion coefficients for calcium and the buffer are denoted by D_{Ca} and D_M (in units of $(\mu m^2/msec)$), respectively. Calcium ions are extruded from the cable via a high-affinity calcium pump where P_m is the membrane pump parameter $(\mu m/msec)$, K_p (μM) represents the pump dissociation constant and the factor $4/d$ is the surface area-to-volume ratio for a cylinder of diameter d. Calcium entry into the cable is carried by two sources; the first is the calcium current $\mathcal{I}^{\nu}_{Ca}(x,t;V;Ca)$ flowing through each specific voltage and calcium-dependent calcium channel ν and the second source is the calcium current through the activation of the NMDA receptors $\mathcal{I}^{\mathrm{NMDA}}_{\mathrm{Ca}}(x,t;V;Ca)$. The ratio $2/\mathcal{F}d$ ensures that the current density per unit length is converted into a concentration gradient. $\mathcal{F}$ is Faraday's constant (C/mol). The summations over calcium channel type ν and their corresponding hotspot locations x^{ν}_i represent the total calcium influx entering the

cable through all calcium-permeable channels.

The calcium reaction-diffusion system can be linearized using the rapid buffer approximation (Iannella & Tanaka, 2006; Zador & Koch, 1994) where in the presence of a fast buffer and under the condition that the calcium concentration is much lower than the pump dissociation constant K_d (i.e., $[Ca]_i \ll K_d$). it has a formal equivalence to the cable equation, allowing the reaction-diffusion system to be reduced to a single partial differential equation (PDE), since assuming a much larger pump dissociation constant than the calcium concentration, the pump behaves linearly;

$$\lim_{[Ca]_i \ll K_d} \frac{4P_m}{d} K_p \frac{[Ca]_i}{[Ca]_i + K_p} \rightarrow \frac{4P_m [Ca]_i}{d}.$$

and when the buffer reaches equilibrium much faster than the diffusion of calcium, this permits the application of the chain rule, leading to the following expression between $[Ca]_i$ and $[M]$:

$$\frac{\partial [M]}{\partial t} = \frac{\partial [M]}{\partial [Ca]_i} \frac{\partial [Ca]_i}{\partial t} = \frac{\mathcal{B}_M^T K_d}{([Ca]_i + K_p)^2} \frac{\partial [Ca]_i}{\partial t}.$$

This allows the calcium reaction-diffusion system for calcium to be reduced to a single equation, namely

$$\begin{aligned} \frac{d(1+\beta)}{4P_m} \frac{\partial [Ca]_i}{\partial t} &= \frac{d(D_{Ca} + \beta D_M)}{4P_m} \frac{\partial^2 [Ca]_i}{\partial x^2} \\ &- [Ca]_i + \sum_{\nu=1}^{s} \sum_{i=1}^{N_\nu} \frac{\mathcal{I}_{Ca}^{\nu}(x,t;V)}{2\mathcal{F}P_m} \delta(x - x_i^{\nu}), \\ &+ \sum_{i=1}^{N_{\text{NMDA}}} \frac{\mathcal{I}_{\text{Ca}}^{\text{NMDA}}(x,t;V;Ca)}{2\mathcal{F}P_m} \delta(x - x_i^{\text{NMDA}}) \end{aligned}$$

where $\beta = \mathcal{B}_M^T / K_d$. This approximation to calcium dynamics allows the system of reaction-diffusion equations can be reduced to the following set of equations, mathematically described by the following system of reaction-diffusion equations given by,

$$\begin{aligned} C_m \frac{\partial V}{\partial t} &= \frac{d}{4\rho_i} \frac{\partial^2 V}{\partial x^2} + g_\ell (V_\ell - V) \\ &+ \sum_{\mu=1}^{k} \sum_{i=1}^{N_\mu} I_{ion}^{\mu}(x,t;V;Ca) \delta(x - x_i^{\mu}) \\ &+ \sum_{i=1}^{N_{\text{AMPA}}} I^{\text{AMPA}}(x,t;V) \delta(x - x_i^{\text{AMPA}}) \\ &+ \sum_{i=1}^{N_{\text{NMDA}}} I^{\text{NMDA}}(x,t;V;Ca) \delta(x - x_i^{\text{NMDA}}) \\ &+ \sum_{i=1}^{N_{\text{GABA}}} I^{\text{GABA}}(x,t;V) \delta(x - x_i^{\text{GABA}}) + \bar{I}_A(x,t) \end{aligned} \tag{4}$$

$$\begin{aligned} \tau_{Ca} \frac{\partial [Ca]_i}{\partial t} &= \lambda_{Ca}^2 \frac{\partial^2 [Ca]_i}{\partial x^2} - [Ca]_i \\ &+ \sum_{\nu=1}^{s} \sum_{i=1}^{N_\nu} \frac{\mathcal{I}_{Ca}^{\nu}(x,t;V)}{2\mathcal{F}P_m} \delta(x - x_i^{\nu}), \\ &+ \sum_{i=1}^{N_{\text{NMDA}}} \frac{\mathcal{I}_{\text{Ca}}^{\text{NMDA}}(x,t;V;Ca)}{2\mathcal{F}P_m} \delta(x - x_i^{\text{NMDA}}), \end{aligned} \tag{5}$$

where we have defined $\tau_{Ca} = d(1+\beta)/(4P_m)$, $\lambda_{Ca} = \sqrt{d(D_{Ca} + \beta D_M)/4P_m}$ and $\beta = \mathcal{B}_M^T / K_p$.

By rewriting Eqns. (4) and (5) in terms of dimensionless variables by introducing the membrane resistivity $R_m = 1/g_\ell$ (Ωcm^2), the dimensionless membrane potential $\Phi(x,t) = V(x,t)/U_{peak}$ (U_{peak} is a voltage reference value typically taken to be the peak value of the membrane potential, namely the maximal value of an action potential), a dimensionless concentration $\Phi_{Ca} = [Ca]_i / [Ca]_{ref}$ where $[Ca]_{ref}$ is some pre-specified non-zero reference concentration. The dimensionless space and time variables are $X = x/\lambda$ and $T = t/\tau_m$, respectively, where the space constant is given by $\lambda = \sqrt{R_m d / 4\rho_i}$ (cm) and $\tau_m = R_m C_m$ (msec) is the membrane time constant. For the calcium component, Eqn. (4) is transformed through the introduction of the dimensionless space and time variables are defined as $X_{Ca} = x/\lambda_{Ca}$ and $T_{Ca} = t/\tau_{Ca}$, where λ_{Ca} and τ_{Ca} are the corresponding space and time constants for calcium, one can rewrite the above system of Eqns. (4) and (5) into the following dimensionless system of cable equations,

$$\begin{aligned} \frac{\partial \Phi}{\partial T} &= \frac{\partial^2 \Phi}{\partial X^2} - \Phi \\ &+ \frac{R_m}{\lambda} \sum_{\mu=1}^{k} \sum_{i=1}^{N_\mu} I_{ion}^{\mu}(X,T;\Phi;\Phi^{Ca}) \delta(X - X_i^{\mu}) \end{aligned}$$

$$+\frac{R_m}{\lambda}\sum_{i=1}^{N_{\text{AMPA}}} I^{\text{AMPA}}(X,T;\Phi)\delta(X-X_i^{\text{AMPA}})$$
$$+\frac{R_m}{\lambda}\sum_{i=1}^{N_{\text{NMDA}}} I^{\text{NMDA}}(X,T;\Phi;\Phi^{Ca})\delta(X-X_i^{\text{NMDA}})$$
$$+\frac{R_m}{\lambda}\sum_{i=1}^{N_{\text{GABA}}} I^{\text{GABA}}(X,T;\Phi)\delta(X-X_i^{\text{GABA}})$$
$$+\frac{I_A(X,T)}{U_{peak}} \tag{6}$$

and

$$\frac{\partial\Phi^{Ca},\Phi^{Ca}}{\partial T_{Ca}} = \frac{\partial^2\Phi^{Ca}}{\partial X_{Ca}^2} - \Phi^{Ca}$$
$$+\mathcal{N}_1\sum_{\nu=1}^{s}\sum_{i=1}^{N_\nu}\mathcal{I}_{Ca}^{\nu}(X_{Ca},t;\Phi;\Phi^{Ca})\delta(X_{ca}-X_{Ca,i}^{\nu})$$
$$+\mathcal{N}_1\sum_{i=1}^{N_{NMDA}}\mathcal{I}_{Ca}^{\nu}(X_{Ca},t;\Phi;\Phi^{Ca})\delta(X_{ca}-X_{Ca,i}^{NMDA}), \tag{7}$$

where we have used the following property of the Dirac delta function, $\delta(\Lambda X) = \delta(X)/\Lambda$. The second equation is the chemical analogue of the cable equation, where the constant $\mathcal{N}_1 = U_{peak}/(2\lambda_{Ca}\mathcal{F}P_m[Ca]_{ref})$, noting that the normalization of calcium by some peak concentration is not possible since the peak concentration is not known a priori. A reasonable choice for $[Ca]_{ref}$ could be the external calcium concentration at rest, i.e., $[Ca]_{ref} = [Ca]_0 = 2\,mM$, the applied current is $I_A = R_m\bar{I}_A$, $X_i^{\mu} = x_i^{\mu}/\lambda$ and $X_{Ca,i}^{\mu} = x_i^{\mu}/\lambda_{Ca}$ denotes the corresponding location of the i^{th} hotspot for channel μ in the cable and chemical cable, respectively. One should note that although the electrotonic location of hotspots occurring in the dimensionless cable and those (chemicotonic locations) in the dimensionless chemical counterpart differ, they each represent the same physical location x in the continuous cable. Here, we assume a finite cable of length $L = \ell/\lambda$ and constant diameter where the initial conditions of the entire system are at rest. The summation appearing in Eqn. (6) represents the sum over all voltage-dependent ionic current sources (noting that some channels can also be calcium-dependent) and is given by

$$\sum_{\mu=1}^{k}\sum_{i=1}^{N_\mu} I_{\text{ion}}^{\mu}(X,T;\Phi;,\Phi^{Ca})\delta(X-X_i^{\mu}) =$$
$$\sum_{i=1}^{N_{\text{Na}}} I^{\text{Na}}(X,T;\Phi)\delta(X-X_i^{\text{Na}})$$
$$+\sum_{j=1}^{N_{\text{K}}} I^{\text{K}}(X,T;\Phi)\delta(X-X_j^{\text{K}})$$
$$+\sum_{l=1}^{N_{\text{K(A)}}} I^{\text{K(A)}}(X,T;\Phi)\delta(X-X_l^{\text{K(A)}})$$
$$+\sum_{m=1}^{N_{\text{Ca(T)}}} I^{\text{Ca(T)}}(X,T;\Phi;\Phi^{Ca})\delta(X-X_m^{\text{Ca(T)}})$$
$$+\sum_{p=1}^{N_{\text{Ca(HVA)}}} I^{\text{Ca(HVA)}}(X,T;\Phi;\Phi^{Ca})\delta(X-X_p^{\text{Ca(HVA)}}),$$

while the corresponding term in Eqn. (6) indicates the sum over all voltage gated calcium channels.

$$\sum_{\nu=1}^{s}\sum_{i=1}^{N_\nu} I_{\text{Ca}}^{\nu}(X_{\text{Ca}},T_{\text{Ca}};\Phi)\delta(X_{\text{Ca}}-X_{\text{Ca},i}^{\nu}) =$$
$$\sum_{m=1}^{N_{\text{Ca(T)}}} I^{\text{Ca(T)}}(X_{\text{Ca}},T_{\text{Ca}};\Phi;\Phi^{Ca})\delta(X_{\text{Ca}}-X_{\text{Ca},m}^{\text{Ca(T)}})$$
$$+\sum_{p=1}^{N_{\text{Ca(HVA)}}} I^{\text{Ca(HVA)}}(X_{\text{Ca}},T_{\text{Ca}};\Phi;\Phi^{Ca})$$
$$\times\delta(X_{\text{Ca}}-X_{\text{Ca},p}^{\text{Ca(HVA)}}),$$

where each ionic current is given by the following general form,

$$I_{\text{ion}}^{\mu}(X_i,T;\Phi,\Phi_{\text{Ca}}) = \varepsilon g^{\mu*}\mathcal{N}^{\mu*}(X_i)\,(m^{\mu}[\Phi_i])^p$$
$$\times(h^{\mu}[\Phi_i])^q\,\mathcal{F}^{\mu}(\Phi_i,\Phi_i^{\text{Ca}}),$$

where μ denotes the type of ion channel, $X_i = X_i^{\mu}$ corresponds to the electrotonic position of the i^{th} hotspot of channel μ, $\varepsilon << 1$ is a factor scaling the "whole-cell" macroscopic transmembrane current density into spatially discrete ion channel clusters, the single channel conductance id denoted by $g^{\mu*}$, $\mathcal{N}^{\mu*}(X_i) = \theta^{\mu}(X_i)/\pi d$ has units of $(cm)^{-1}$ and represents the number of channels per unit length, $\theta^{\mu}(X_i)$ denotes the number of channels in the i^{th} hotspot of channel μ, $m^{\mu}(\Phi)$ and $h^{\mu}(\Phi)$ are the activation and inactivation variables of channel μ, respectively, p and q are exponents, and $\mathcal{F}^{\mu}(\Phi_i,\Phi_i^{\text{Ca}})$ represents the voltage and/or calcium current dependence of channel μ, and $\Phi_{\mu} = V_{\mu}/U_{peak}$ is the dimensionless equilibrium potential where V_{μ} is the usual equilibrium

potential (mV) of channel μ.

One can now transform our general system of cable equations into a system of nonlinear integral equations using the same techniques as described by (Iannella & Tanaka, 2006 2007),

$$\begin{aligned}\Phi(X,T) &= \Psi(X,T) \\ &+ \Psi^{\mathrm{AMPA}}(X,T) + \Psi^{\mathrm{GABA}}(X,T) + \Psi^{\mathrm{NMDA}}(X,T) \\ &+ \varepsilon\frac{R_m}{\lambda}\int_0^T \sum_{\mu=1}^{k}\sum_{i=1}^{N_\mu} f^{\mu}\Big[\Phi_i(s),\Phi_i^{\mathrm{Ca}}(s)\Big] \\ &\qquad \times G(X,X_i^{\mu};T-s)ds, \qquad (8)\end{aligned}$$

$$\begin{aligned}&\Phi^{Ca}(X_{Ca},T_{Ca}) = \\ &\Psi_{Ca}(X_{Ca},T_{Ca}) + \Psi_{Ca}^{\mathrm{NMDA}}(X_{Ca},T_{Ca}) \\ &+ \varepsilon\aleph_1\int_0^{T_{\mathrm{Ca}}}\sum_{i=1}^{N_{Ca(T)}} \mathfrak{F}^{Ca(T)}\Big[\Phi_i(s),\Phi_i^{Ca}(s)\Big] \\ &\qquad \times G\left(X_{Ca},X_{Ca,i};T_{Ca}-s\right)ds \\ &+ \varepsilon\aleph_1\int_0^{T_{Ca}}\sum_{i=1}^{N_{Ca(HVA)}} \mathfrak{F}^{Ca(HVA)}\Big[\Phi_i(s),\Phi_i^{Ca}(s)\Big] \\ &\qquad \times G\left(X_{Ca},X_{Ca,i};T_{Ca}-s\right)ds, \qquad (9)\end{aligned}$$

where

$$\Psi(X,T) = \int_0^T\int_0^L \frac{I_A(Y,s)}{U_{peak}}G(X,Y;T-s)dYds$$

$$\begin{aligned}&\Psi^{\mathrm{AMPA}}(X,T) = \\ &\varepsilon\frac{R_m}{\lambda}\int_0^T\sum_{i=1}^{N_{\mathrm{AMPA}}} f^{\mathrm{AMPA}}[\Phi_i(s)] \\ &\qquad \times G(X,X_i^{\mathrm{AMPA}};T-s)ds\end{aligned}$$

$$\begin{aligned}&\Psi^{\mathrm{GABA}}(X,T) = \\ &\varepsilon\frac{R_m}{\lambda}\int_0^T\sum_{i=1}^{N_{\mathrm{GABA}}} f^{\mathrm{GABA}}[\Phi_i(s)] \\ &\qquad \times G(X,X_i^{\mathrm{GABA}};T-s)ds\end{aligned}$$

$$\begin{aligned}&\Psi^{\mathrm{NMDA}}(X,T) = \\ &\varepsilon\frac{R_m}{\lambda}\int_0^T\sum_{i=1}^{N_{\mathrm{NMDA}}} f^{\mathrm{NMDA}}[\Phi_i(s)] \\ &\qquad \times G(X,X_i^{\mathrm{NMDA}};T-s)ds\end{aligned}$$

$$\begin{aligned}&\Psi_{\mathrm{Ca}}^{\mathrm{Ca}}(X_{\mathrm{Ca}},T_{\mathrm{Ca}}) = \\ &\int_0^L G(X_{\mathrm{Ca}},Y_{\mathrm{Ca}};T_{\mathrm{Ca}})\Phi^{\mathrm{Ca}}(Y_{\mathrm{Ca}},0)\,dY_{\mathrm{Ca}}\end{aligned}$$

$$\begin{aligned}&\Psi_{\mathrm{Ca}}^{\mathrm{NMDA}}(X_{\mathrm{Ca}},T_{\mathrm{Ca}}) = \\ &\varepsilon\mathcal{N}_1\int_0^{T_{\mathrm{Ca}}}\sum_{i=1}^{N_{\mathrm{NMDA}}} f_{\mathrm{Ca}}^{\mathrm{NMDA}}\Big[\Phi_i(s),\Phi_i^{\mathrm{Ca}}(s)\Big] \\ &\qquad \times G\left(X_{\mathrm{Ca}},X_{\mathrm{Ca},i};T_{\mathrm{Ca}}-s\right)ds\end{aligned}$$

$$\aleph_1 = \frac{U_{peak}}{2\lambda_{Ca}\mathcal{F}P_m[Ca]_{ref}}.$$

Solutions can then be derived by performing a perturbative expansion for $\Phi(X,T)$ and $\Phi^{Ca}(X_{Ca},T_{Ca})$, respectively.

$$\begin{aligned}\Phi(X,T) &= \Phi_0(X,T) + \varepsilon\Phi_1(X,T) + \varepsilon^2\Phi_2(X,T) \\ &\quad + \varepsilon^3\Phi_3(X,T) + O(\varepsilon^4)\end{aligned}$$

$$\begin{aligned}\Phi^{Ca}(X_{Ca},T_{Ca}) &= \Phi_0^{Ca}(X_{Ca},T_{Ca}) + \varepsilon\Phi_1^{Ca}(X_{Ca},T_{Ca}) \\ &+ \varepsilon^2\Phi_2^{Ca}(X_{Ca},T_{Ca}) + \varepsilon^3\Phi_3^{Ca}(X_{Ca},T_{Ca}) + O(\varepsilon^4).\end{aligned}$$

After some algebra and collecting like terms in powers of ε, we arrive at

$$\begin{aligned}\Phi_1(X,T) &= \frac{R_m}{\lambda}\sum_{\mu=1}^{k}\sum_{i=1}^{N_\mu}\int_0^T G(X,X_i^{\mu};T-s) \\ &\qquad \times f^{\mu}\Big[\Phi_{0i}(s),\Phi_{0i}^{Ca}(s)\Big]ds \\ &+ \frac{R_m}{\lambda}\sum_{i=1}^{N_{\mathrm{AMPA}}}\int_0^T G(X,X_i^{\mathrm{AMPA}};T-s) \\ &\qquad \times f^{\mathrm{AMPA}}[\Phi_{0i}(s)]\,ds \\ &+ \frac{R_m}{\lambda}\sum_{i=1}^{N_{\mathrm{GABA}}}\int_0^T G(X,X_i^{\mathrm{GABA}};T-s) \\ &\qquad \times f^{\mathrm{GABA}}[\Phi_{0i}(s)]\,ds \\ &+ \frac{R_m}{\lambda}\sum_{i=1}^{N_{\mathrm{NMDA}}}\int_0^T G(X,X_i^{\mathrm{NMDA}};T-s) \\ &\qquad \times f^{\mathrm{NMDA}}[\Phi_{0i}(s)]\,ds\end{aligned}$$

$$\begin{aligned}\Phi_2(X,T) &= \frac{R_m}{\lambda}\sum_{\mu=1}^{k}\sum_{i=1}^{N_\mu}\int_0^T G(X,X_i^{\mu};T-s) \\ &\times\left\{\frac{\partial f^{\mu}}{\partial\Phi}\Big[\Phi_{0i}(s),\Phi_{0i}^{Ca}(s)\Big]\Phi_{1i}(s)\right. \\ &\quad \left.+\frac{\partial f^{\mu}}{\partial\Phi^{Ca}}\Big[\Phi_{0i}(s),\Phi_{0i}^{Ca}(s)\Big]\Phi_{1i}^{Ca}(s)\right\}ds\end{aligned}$$

$$
\begin{aligned}
&+\frac{R_m}{\lambda}\sum_{i=1}^{N_{\mathrm{AMPA}}}\int_0^T G(X,X_i^{\mathrm{AMPA}};T-s)\\
&\qquad\times\frac{\partial f^{\mathrm{AMPA}}}{\partial\Phi}[\Phi_{0i}(s)]\,\Phi_{1i}(s)ds\\
&+\frac{R_m}{\lambda}\sum_{i=1}^{N_{\mathrm{GABA}}}\int_0^T G(X,X_i^{\mathrm{GABA}};T-s)\\
&\qquad\times\frac{\partial f^{\mathrm{GABA}}}{\partial\Phi}[\Phi_{0i}(s)]\,\Phi_{1i}(s)ds\\
&+\frac{R_m}{\lambda}\sum_{i=1}^{N_{\mathrm{NMDA}}}\int_0^T G(X,X_i^{\mathrm{NMDA}};T-s)\\
&\qquad\times\frac{\partial f^{\mathrm{NMDA}}}{\partial\Phi}[\Phi_{0i}(s)]\,\Phi_{1i}(s)ds
\end{aligned}
$$

$$
\begin{aligned}
\Phi_3(X,T)=\frac{R_m}{\lambda}\sum_{\mu=1}^{k}\sum_{i=1}^{N_\mu}\int_0^T G(X,X_i^{\mu};T-s)\\
\times\Big\{\frac{\partial f^{\mu}}{\partial\Phi}\Big[\Phi_{0i}(s),\Phi_{0i}^{Ca}(s)\Big]\Phi_{2i}(s)\\
+\frac{\partial f^{\mu}}{\partial\Phi^{Ca}}\Big[\Phi_{0i}(s),\Phi_{0i}^{Ca}(s)\Big]\Phi_{2i}^{Ca}(s)\\
+\frac{1}{2}\frac{\partial^2 f^{\mu}}{\partial\Phi^2}\Big[\Phi_{0i}(s),\Phi_{0i}^{Ca}(s)\Big]\Phi_{1i}^2(s)\\
+\frac{\partial^2 f^{\mu}}{\partial\Phi\partial\Phi^{Ca}}\Big[\Phi_{0i}(s),\Phi_{0i}^{Ca}(s)\Big]\Phi_{1i}(s)\Phi_{1i}^{Ca}(s)\\
+\frac{1}{2}\frac{\partial^2 f^{\mu}}{\partial\Phi^{Ca}\partial\Phi^{Ca}}\Big[\Phi_{0i}(s),\Phi_{0i}^{Ca}(s)\Big]\\
\qquad\times\Phi_{1i}^{Ca}(s)\Phi_{1i}^{Ca}(s)\Big\}\\
+\frac{R_m}{\lambda}\sum_{i=1}^{N_{\mathrm{AMPA}}}\int_0^T G(X,X_i^{\mathrm{AMPA}};T-s)\\
\times\Big\{\frac{\partial f^{\mathrm{AMPA}}}{\partial\Phi}[\Phi_{0i}(s)]\,\Phi_{2i}(s)\\
+\frac{1}{2}\frac{\partial^2 f^{\mathrm{AMPA}}}{\partial\Phi^2}[\Phi_{0i}(s)]\,\Phi_{1i}^2(s)\Big\}ds\\
+\frac{R_m}{\lambda}\sum_{i=1}^{N_{\mathrm{GABA}}}\int_0^T G(X,X_i^{\mathrm{GABA}};T-s)\\
\times\Big\{\frac{\partial f^{\mathrm{GABA}}}{\partial\Phi}[\Phi_{0i}(s)]\,\Phi_{2i}(s)\\
+\frac{1}{2}\frac{\partial^2 f^{\mathrm{GABA}}}{\partial\Phi^2}[\Phi_{0i}(s)]\,\Phi_{1i}^2(s)\Big\}ds\\
+\frac{R_m}{\lambda}\sum_{i=1}^{N_{\mathrm{NMDA}}}\int_0^T G(X,X_i^{\mathrm{NMDA}};T-s)\\
\times\Big\{\frac{\partial f^{\mathrm{NMDA}}}{\partial\Phi}[\Phi_{0i}(s)]\,\Phi_{2i}(s)\\
+\frac{1}{2}\frac{\partial^2 f^{\mathrm{NMDA}}}{\partial\Phi^2}[\Phi_{0i}(s)]\,\Phi_{1i}^2(s)\Big\}ds
\end{aligned}
\tag{10}
$$

and

$$
\begin{aligned}
&\Phi_1^{Ca}(X_{Ca},T_{Ca})=\\
&\aleph_1\sum_{i=1}^{N_{Ca(HVA)}}\int_0^{T_{Ca}} G(X_{Ca},X_{Ca,i};T_{Ca}-s)\\
&\qquad\times\mathfrak{F}^{Ca(HVA)}\Big[\Phi_{0i}(s),\Phi_{0i}^{Ca}(s)\Big]ds\\
&+\aleph_1\sum_{i=1}^{N_{\mathrm{AMPA}}}\int_0^T G(X_{Ca},X_i^{\mathrm{AMPA}};T_{Ca}-s)\\
&\qquad\times f^{\mathrm{AMPA}}[\Phi_{0i}(s)]\,ds\\
&+\aleph_1\sum_{i=1}^{N_{\mathrm{GABA}}}\int_0^T G(X_{Ca},X_i^{\mathrm{GABA}};T_{Ca}-s)\\
&\qquad\times f^{\mathrm{GABA}}[\Phi_{0i}(s)]\,ds\\
&+\aleph_1\sum_{i=1}^{N_{\mathrm{NMDA}}}\int_0^T G(X_{Ca,i},X^{\mathrm{NMDA}};T_{Ca}-s)\\
&\qquad\times f^{\mathrm{NMDA}}[\Phi_{0i}(s)]\,ds\\
&\Phi_2^{Ca}(X_{Ca},T_{Ca})=\\
&\aleph_1\sum_{i=1}^{N_{Ca(HVA)}}\int_0^{T_{Ca}} G(X_{Ca},X_{Ca,i};T_{Ca}-s)\\
&\qquad\times\Big\{\frac{\partial\mathfrak{F}^{Ca(HVA)}}{\partial\Phi}\Big[\Phi_{0i}(s),\Phi_{0i}^{Ca}(s)\Big]\Phi_{1i}(s)\\
&\qquad+\frac{\partial\mathfrak{F}^{Ca(HVA)}}{\partial\Phi^{Ca}}\Big[\Phi_{0i}(s),\Phi_{0i}^{Ca}(s)\Big]\Phi_{1i}^{Ca}(s)\Big\}ds\\
&+\aleph_1\sum_{i=1}^{N_{\mathrm{AMPA}}}\int_0^T G(X_{Ca},X_{Ca,i}^{\mathrm{AMPA}};T_{Ca}-s)\\
&\qquad\times\frac{\partial f^{\mathrm{AMPA}}}{\partial\Phi}[\Phi_{0i}(s)]\,\Phi_{1i}(s)ds\\
&+\aleph_1\sum_{i=1}^{N_{\mathrm{GABA}}}\int_0^T G(X_{Ca},X_{Ca,i}^{\mathrm{GABA}};T_{Ca}-s)\\
&\qquad\times\frac{\partial f^{\mathrm{GABA}}}{\partial\Phi}[\Phi_{0i}(s)]\,\Phi_{1i}(s)ds\\
&+\aleph_1\sum_{i=1}^{N_{\mathrm{NMDA}}}\int_0^T G(X_{Ca},X_{Ca,i}^{\mathrm{NMDA}};T_{Ca}-s)\\
&\qquad\times\frac{\partial f^{\mathrm{NMDA}}}{\partial\Phi}[\Phi_{0i}(s)]\,\Phi_{1i}(s)ds
\end{aligned}
$$

$$
\begin{aligned}
&\Phi_3^{Ca}(X_{Ca}, T_{Ca}) = \\
&\aleph_1 \sum_{i=1}^{N_{Ca(HVA)}} \int_0^{T_{Ca}} G(X_{Ca}, X_{Ca,i}; T_{Ca} - s) \\
&\times \left\{ \frac{\partial \mathfrak{F}^{Ca(HVA)}}{\partial \Phi} \left[\Phi_{0i}(s), \Phi_{0i}^{Ca}(s)\right] \Phi_{2i}(s) \right. \\
&+ \frac{\partial \mathfrak{F}^{Ca(HVA)}}{\partial \Phi^{Ca}} \left[\Phi_{0i}(s), \Phi_{0i}^{Ca}(s)\right] \Phi_{2i}^{Ca}(s) \\
&+ \frac{1}{2} \frac{\partial^2 \mathfrak{F}^{Ca(HVA)}}{\partial \Phi^2} \left[\Phi_{0i}(s), \Phi_{0i}^{Ca}(s)\right] \Phi_{1i}(s) \Phi_{1i}(s) \\
&+ \frac{\partial^2 \mathfrak{F}^{Ca(HVA)}}{\partial \Phi \partial \Phi^{Ca}} \left[\Phi_{0i}(s), \Phi_{0i}^{Ca}(s)\right] \Phi_{1i}(s) \Phi_{1i}^{Ca}(s) \\
&\left. + \frac{1}{2} \frac{\partial^2 \mathfrak{F}^{Ca(HVA)}}{\partial \Phi^{Ca} \partial \Phi^{Ca}} \left[\Phi_{0i}(s), \Phi_{0i}^{Ca}(s)\right] \Phi_{1i}^{Ca}(s) \Phi_{1i}^{Ca}(s) \right\} ds \\
&+ \aleph_1 \sum_{i=1}^{N_{\mathrm{AMPA}}} \int_0^{T} G(X_{Ca}, X_{Ca,i}^{\mathrm{AMPA}}; T_{Ca} - s) \\
&\times \left\{ \frac{\partial f^{\mathrm{AMPA}}}{\partial \Phi} \left[\Phi_{0i}(s)\right] \Phi_{2i}(s) \right. \\
&\qquad \left. + \frac{1}{2} \frac{\partial^2 f^{\mathrm{AMPA}}}{\partial \Phi^2} \Phi_{1i}^2(s) \right\} \\
&+ \aleph_1 \sum_{i=1}^{N_{\mathrm{GABA}}} \int_0^{T} G(X_{Ca}, X_{Ca,i}^{\mathrm{GABA}}; T_{Ca} - s) \\
&\times \left\{ \frac{\partial f^{\mathrm{GABA}}}{\partial \Phi} \left[\Phi_{0i}(s)\right] \Phi_{2i}(s) \right. \\
&\qquad \left. + \frac{1}{2} \frac{\partial^2 f^{\mathrm{GABA}}}{\partial \Phi^2} \Phi_{1i}^2(s) \right\} ds \\
&+ \aleph_1 \sum_{i=1}^{N_{\mathrm{NMDA}}} \int_0^{T} G(X_{Ca}, X_{Ca,i}^{\mathrm{NMDA}}; T_{Ca} - s) \\
&\times \left\{ \frac{\partial f^{\mathrm{NMDA}}}{\partial \Phi} \Phi_{2i}(s) \right. \\
&\qquad \left. + \frac{1}{2} \frac{\partial^2 f^{\mathrm{NMDA}}}{\partial \Phi^2} \Phi_{1i}^2(s) \right\} ds, \qquad (11)
\end{aligned}
$$

where $X_i = X_i^{\mu}$ represents the electrotonic position of the i^{th} μ channel hotspot and $X_{Ca,i}$ denotes the chemicotonic position of the i^{th} HVA calcium channel hotspot.

The expressions Eqns (8-11) present the perturbative solutions for the general case when the voltage and calcium systems are coupled via their dependence through the current dependence of channel μ, namely $\mathcal{F}^{\mu}(\Phi_i, \Phi_i^{\mathrm{Ca}})$. These expressions are needed when the current dependence of the high-voltage activated L-type and low-voltage activated T-type calcium channels are dependent on calcium and voltage and any functional dependence from input currents generated through AMPA, GABA, and NMDA receptors by synaptic inputs.

For the illustrative purposes of this study, we will consider the case where there is only voltage (no explicit calcium) dependence in the mathematical representation of each respective ion channel. Similar to many previous studies, ionic currents are expressed as,

$$
\begin{aligned}
I_{\mathrm{ion}}^{\mu}(X_i, T; \Phi) = \varepsilon g^{\mu *} \mathcal{N}^{\mu *}(X_i) \left(m^{\mu}[\Phi_i]\right)^p \\
\times \left(h^{\mu}[\Phi_i]\right)^q (\Phi_{\mu} - \Phi).
\end{aligned}
$$

When presynaptic stimulation occurs at time T_j, this can generate a current through any present AMPA receptor hotspots

$$
\begin{aligned}
I^{\mathrm{AMPA}}(X_i^{\mathrm{AMPA}}, T; \Phi) = \varepsilon g^{\mathrm{AMPA}} \mathcal{N}^{\mathrm{AMPA}}(X_i^{\mathrm{AMPA}}) \\
\times \bar{\mathfrak{g}}_{\mathrm{AMPA}}(T - T_j) H(T - T_j)(\Phi_{\mathrm{AMPA}}^{\mathrm{rev}} - \Phi).
\end{aligned}
$$

Similarly, GABAergic inputs generate hyperpolarizing or inhibitory input currents through their corresponding receptor hotspots given by,

$$
\begin{aligned}
I^{\mathrm{GABA}}(X_i^{\mathrm{GABA}}, T; \Phi) = \varepsilon g^{\mathrm{GABA}} \mathcal{N}^{\mathrm{GABA}}(X_i^{\mathrm{GABA}}) \\
\times \bar{\mathfrak{g}}_{\mathrm{GABA}}(T - T_j) H(T - T_j)(\Phi_{\mathrm{GABA}}^{\mathrm{rev}} - \Phi),
\end{aligned}
$$

while the NMDA receptor-generated current and the corresponding calcium current through this receptor is given by

$$
\begin{aligned}
I^{\mathrm{NMDA}}(X_i^{\mathrm{NMDA}}, T; \Phi) = \\
\varepsilon g^{\mathrm{NMDA}} \mathcal{N}^{\mathrm{NMDA}}(X_i^{\mathrm{NMDA}}) \bar{\mathfrak{g}}_{\mathrm{NMDA}}(T - T_j) \\
\times H(T - T_j) B(\Phi)(\Phi_{\mathrm{NMDA}}^{\mathrm{rev}} - \Phi)
\end{aligned}
$$

$$
\begin{aligned}
I_{\mathrm{Ca}}^{\mathrm{NMDA}}(X_{\mathrm{Ca}}, T_{\mathrm{Ca}}; \Phi) = \varepsilon g^{\mathrm{NMDA}} \mathcal{N}^{\mathrm{NMDA}}(X_{\mathrm{Ca},i}) \\
\times \bar{\mathfrak{g}}_{\mathrm{NMDA}}(T_{\mathrm{Ca}} - T_{\mathrm{Ca},j}) H(T_{\mathrm{Ca}} - T_{\mathrm{Ca},j}) \\
\times B(\Phi)(\Phi_{\mathrm{Ca}}^{\mathrm{rev}} - \Phi),
\end{aligned}
$$

where X_i^{μ}, X_i^{AMPA}, X_i^{GABA}, and X_i^{NMDA} represents the electrotonic positions of the i^{th} μ channel, AMPA, GABA, and NMDA receptor hotspots, respectively. Similarly, $X_{\mathrm{Ca,i}}^{\nu}$ and $X_{\mathrm{Ca},i}^{\mathrm{NMDA}}$ denotes the corresponding chemicotonic positions of calcium currents generated by the i^{th} ν-type calcium channel and NMDA

receptor hotspots, respectively. Here, the single channel conductance for AMPA is denoted by g^{AMPA}, $\mathcal{N}^{\text{AMPA}}(X_i^{\text{AMPA}}) = \theta^{\text{AMPA}}(X_i^{\text{AMPA}})/\pi d$ corresponds to the number of AMPA receptors per unit length (cm^{-1}), θ^{AMPA} represents the number of AMPA receptors in the i^{th} AMPA receptor hotspot, $\bar{g}_{\text{AMPA}}(T)$ is the corresponding conductance change of the AMPA receptor. Likewise, the single channel conductance for GABA is g^{GABA}, where $\mathcal{N}^{\text{GABA}}(X_i^{\text{GABA}}) = \theta^{\text{GABAA}}(X_i^{\text{GABA}})/\pi d$ is the number of GABA receptors per unit length (cm^{-1}), θ^{GABA} represents the number of GABA receptors in the i^{th} GABA receptor hotspot, $\bar{g}_{\text{GABA}}(T)$ is the corresponding conductance change of the GABA receptor. Similarly, for NMDA, we have g^{NMDA}, $\mathcal{N}^{\text{NMDA}}(X_i^{\text{NMDA}}) = \theta^{\text{NMDA}}(X_i^{\text{NMDA}})/\pi d$ corresponds to the number of NMDA receptors per unit length (cm^{-1}), θ^{NMDA} represents the number of NMDA receptors in the i^{th} NMDA receptor hotspot, $\bar{g}_{\text{NMDA}}(T)$ is the conductance change associated with the NMDA receptor, $H(T)$ denotes the Heaviside step function, $\Phi^{\text{rev}}_{\text{NMDA}}$ and $\Phi^{\text{rev}}_{\text{Ca}}$ are the reversal potentials for NMDA and calcium, respectively, and finally the magnesium block is represented by a nonlinear voltage dependent function $B(\Phi)$ given by (Jahr & Stevens, 1990),

$$B(\Phi) = \frac{1}{1 + \exp(-0.062 U_{\text{peak}}\Phi)[\text{Mg}^{2+}]_0/3.57},$$

where $[\text{Mg}^{2+}]_0$ is the extracellular magnesium concentration.

These choices lead to a system of cable equations where voltage and calcium are uncoupled, and by following the method described in (Iannella & Tanaka, 2007), and applying a perturbative expansion for only $\Phi(X,T)$ (after recasting Eqns. (8) and (9) into the corresponding system of nonlinear Volterra integral equations) one arrives at the following,

$$\begin{aligned}
\Phi_1(X,T) = {} & \frac{R_m}{\lambda}\sum_{\mu=1}^{k}\sum_{i=1}^{N_\mu}\int_0^T G(X, X_i^\mu; T-s) \\
& \times f^{\mu}[\Phi_{0i}(s)]\,ds \\
& + \frac{R_m}{\lambda}\sum_{i=1}^{N_{\text{AMPA}}}\int_0^T G(X, X_i^{\text{AMPA}}; T-s) \\
& \times f^{\text{AMPA}}[\Phi_{0i}(s)]\,ds \\
& + \frac{R_m}{\lambda}\sum_{i=1}^{N_{\text{NMDA}}}\int_0^T G(X, X_i^{\text{NMDA}}; T-s) \\
& \times f^{\text{NMDA}}[\Phi_{0i}(s)]\,ds
\end{aligned}$$

$$\begin{aligned}
\Phi_2(X,T) = {} & \frac{R_m}{\lambda}\sum_{\mu=1}^{k}\sum_{i=1}^{N_\mu}\int_0^T G(X, X_i^\mu; T-s) \\
& \times \frac{\partial f^{\mu}}{\partial \Phi}[\Phi_{0i}(s)]\,\Phi_{1i}(s)ds, \\
& + \frac{R_m}{\lambda}\sum_{i=1}^{N_{\text{AMPA}}}\int_0^T G(X, X_i^{\text{AMPA}}; T-s) \\
& \times \frac{\partial f^{\text{AMPA}}}{\partial \Phi}[\Phi_{0i}(s)]\,\Phi_{1i}(s)ds, \\
& + \frac{R_m}{\lambda}\sum_{i=1}^{N_{\text{NMDA}}}\int_0^T G(X, X_i^{\text{NMDA}}; T-s) \\
& \times \frac{\partial f^{\text{NMDA}}}{\partial \Phi}[\Phi_{0i}(s)]\,\Phi_{1i}(s)ds
\end{aligned}$$

$$\begin{aligned}
\Phi_3(X,T) = {} & \\
& \frac{R_m}{\lambda}\sum_{\mu=1}^{k}\sum_{i=1}^{N_\mu}\int_0^T G(X, X_i^\mu; T-s) \\
& \times \left\{\frac{\partial f^{\mu}}{\partial \Phi}[\Phi_{0i}(s)]\,\Phi_{2i}(s)\right. \\
& \left. + \frac{1}{2!}\frac{\partial^2 f^{\mu}}{\partial \Phi^2}[\Phi_{0i}(s)]\,\Phi_{1i}^2(s)\right\}ds, \\
& + \frac{R_m}{\lambda}\sum_{i=1}^{N_{\text{AMPA}}}\int_0^T G(X, X_i^{\text{AMPA}}; T-s) \\
& \times \left\{\frac{\partial f^{\text{AMPA}}}{\partial \Phi}[\Phi_{0i}(s)]\,\Phi_{2i}(s)\right. \\
& \left. + \frac{1}{2!}\frac{\partial^2 f^{\text{AMPA}}}{\partial \Phi^2}[\Phi_{0i}(s)]\,\Phi_{1i}^2(s)\right\}ds \\
& + \frac{R_m}{\lambda}\sum_{i=1}^{N_{\text{NMDA}}}\int_0^T G(X, X_i^{\text{NMDA}}; T-s) \\
& \times \left\{\frac{\partial f^{\text{NMDA}}}{\partial \Phi}[\Phi_{0i}(s)]\,\Phi_{2i}(s)\right. \\
& \left. + \frac{1}{2!}\frac{\partial^2 f^{\text{NMDA}}}{\partial \Phi^2}[\Phi_{0i}(s)]\,\Phi_{1i}^2(s)\right\}ds
\end{aligned} \tag{12}$$

and

$$\Phi^{\text{Ca}}(X_{\text{Ca}}, T_{\text{Ca}}) =$$

$$\int_0^{L_{\mathrm{Ca}}} G_{\mathrm{Ca}}(X_{\mathrm{Ca}}, Y_{\mathrm{Ca}}; T_{\mathrm{Ca}})\Phi^{\mathrm{Ca}}(Y_{\mathrm{Ca}}, 0)\, dY_{\mathrm{Ca}}$$
$$+ \aleph_1 \sum_{\nu=1}^{s} \sum_{i=1}^{N_\nu} \int_0^{T_{\mathrm{Ca}}} G_{\mathrm{Ca}}\left(X_{\mathrm{Ca}}, X^{\nu}_{\mathrm{Ca},i}; T_{\mathrm{Ca}} - s\right) \times \mathcal{I}^{\nu}_{\mathrm{Ca}}\left(X^{\nu}_{\mathrm{Ca},i}, s\right) ds$$
$$+ \aleph_1 \sum_{i=1}^{N_{\mathrm{NMDA}}} \int_0^{T_{\mathrm{Ca}}} G_{\mathrm{Ca}}\left(X_{\mathrm{Ca}}, X^{\mathrm{NMDA}}_{\mathrm{Ca},i}; T_{\mathrm{Ca}} - s\right) \times \mathcal{I}^{\mathrm{NMDA}}_{\mathrm{Ca}}\left(X^{\mathrm{NMDA}}_{\mathrm{Ca},i}, s\right) ds. \quad (13)$$

The integral expressions represent convolutions between the Green's function and various functional forms involving zero, first, and higher-order terms of the ionic current and voltage contributions calculated via a regular perturbation expansion.

For the specific case of our voltage-based cable equation, we employ a nonhomogeneous Dirichlet boundary condition at $X = 0$, which implements a nonlinear current clamp with the shape of an action potential, i.e. $\Phi(0, t) = f(t)$. While for impulsive inputs occurring along the cable, we assume that the current clamp at $X = 0$ is set to zero, the corresponding boundary condition for these inputs is equivalent to the killed end condition $\Phi(0, t) = 0$. At the other end of the cable at $X = L$, the sealed-end boundary condition is adopted. Analogously for the calcium-based cable equation, we employ sealed-end boundary conditions at $X_{\mathrm{Ca}} = 0$ ($X = 0$) and $X_{\mathrm{Ca}} = L_{\mathrm{Ca}}$ ($X = L$) since there is no calcium flowing out of each end.

Action potentials from hippocampal and somatosensory pyramidal cells (Larkum et al., 2001; Magee & Johnston, 1997) typically possess an after-depolarising tail and have been shown to participate in synaptic plasticity due to increased calcium influx through NMDA receptors and voltage-gated calcium channels (VGCC) (Isomura & Kato, 1999; Isomura et al., 2002; Kampa et al., 2006; Magee & Johnston, 1997; Metz et al., 2005). These action potentials are modelled as,

$$I_A(0, T) = U_0 \left(10e^{-2T} \sin\left((2\pi/150)T\right) + 67e^{-30T} - 70e^{-60T} + 3e^{-0.625T}\right) H(T).$$

NMDA-derived calcium currents occur from the coincidence between the presynaptic activation of a postsynaptic NMDA receptor hotspot and action potential propagation into a dendritic section. Membrane depolarisation along the dendritic section is used to calculate the resulting calcium profiles. These calcium profiles can then be used to evaluate the change in synaptic weight, where the parameters used in the following sets of simulations were $A = 0.35$, $p_1 = 1$, $p_2 = 1.65$, $p_3 = 3$, $p_4 = 0$, $a_1 = 0.15$, $b_1 = 30$, $a_2 = 0.45$, and $b_2 = 30$ unless stated otherwise.

3. Results

3.1. Spatial dependence of STDP

A landmark experiment illustrated that the STDP learning window is not homogeneous but varies as a function of distance along the length of dendrite where one observes an elongation and increase in the decay time constant of the LTD portion of this window was observed (Froemke et al., 2005). A previous modelling study reproduced this effect using calcium-based plasticity (Iannella et al., 2014) illustrating that the properties and spatial distribution of ion channels influence the profile of the STDP window as a function of location. Here, we demonstrate that our model also exhibits similar changes to the STDP window as a function of distance along the portion of the dendrite as can be observed in **Fig 2**.

Other factors can influence the profile of the resulting STDP window. Studies have illustrated that neuronal morphology can also impact firing properties of neurons (Iannella et al., 2004; Mainen & Sejnowski, 1996; Rall, 1964; Tuckwell, 1988*a*), leading to diverse spatial and temporal calcium profiles along dendrites and this in turn changes calcium-dependent plasticity outcomes. Other factors, like neural excitability, also contribute to these outcomes since changes will impact the amount and location of calcium influx, contributing to whether potentiation or depression occurs. Here, varying the density of calcium ion channels, such as high voltage-activated (L-type) and low voltage-activated (T-type) channels, can lead to changes in calcium profiles and impact the resulting STDP window at that location (Iannella et al., 2014).

3.2. *Heterosynaptic influence: How spatial interactions between synaptic inputs can alter plasticity at the induction site*

Another aspect that is not often discussed, but is gaining increasing interest is the impact of heterosynaptic influences on plasticity outcomes. Typically, heterosynaptic plasticity focuses on how the induction of synaptic plasticity at some dendritic location may change the synaptic efficacy at nearby synapses that are not active during the induction (Chistiakova & Volgushev, 2009). This, however, presents one side to the idea behind *heterosynaptic influences*; significantly, there is another aspect that (we believe) has not been extensively discussed or considered, and that is how other (non-plasticity) inducing synaptic inputs to other locations influence the induction and expression of synaptic plasticity at the site of interest. At first glance, this seems to be the opposite of heterosynaptic plasticity or could even be interpreted as a form of homosynaptic plasticity, here we argue that these two seemingly different situations embrace what we define as *heterosynaptic influence/interaction*, namely how inputs at one or various locations influence the plasticity outcome at the location of interest. Note that this definition captures the notion of both heterosynaptic plasticity and the visa-versa situation of how non-plastic-inducing synaptic inputs impact the expression and outcome of plasticity at the induction site.

(A)

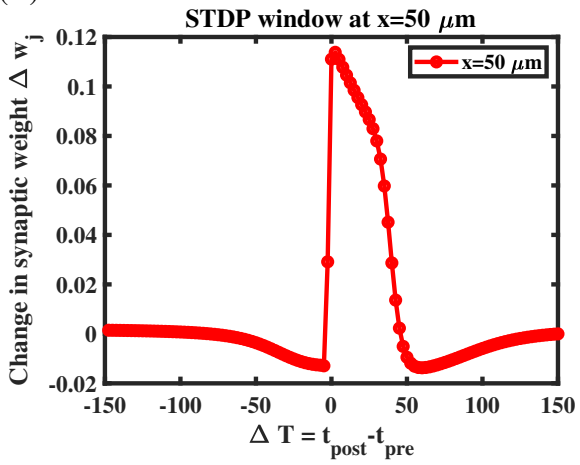

(B)

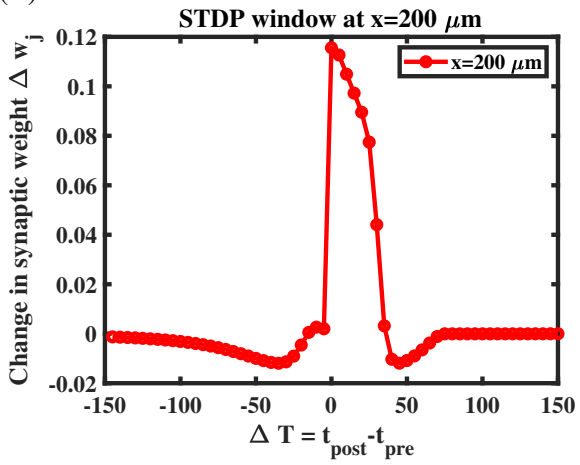

Figure 2: Resulting STDP learning windows taken from two positions **(A)** $x = 50\ \mu m$ and **(B)** $x = 200\ \mu m$ along the cable, respectively. One can observe an increase in the time constant of the LTD portion of the STDP as a function of distance and mimics the location-dependent nature of the STDP window demonstrated from experiment (Froemke et al., 2005). Parameters used for our calcium-basd plasticity model were $A = 0.35$, $p_1 = 1$, $p_2 = 1.65$, $p_3 = 3$, $p_4 = 0$, $a_1 = 0.15$, $b_1 = 30$, $a_2 = 0.45$, and $b_2 = 30$.

To investigate how non-plastic-inducing synaptic inputs impact plasticity, simulations were conducted using the STDP pairing paradigm at a synapse that contains NMDA and an additional short train of spike inputs that activate AMPA receptors in a synaptic location close to the synapse where STDP will be induced. The short train consists of eleven spikes where the middle spike is synchronised with the post-synaptic spike (back-propagating action potential). The frequency of spikes that comprise the short train was 50 Hz. STDP was induced in a synapse located 50 μm from the left boundary and contains NMDA receptors. To find how the short train of inputs impacts the synapse where STDP induction takes place, the location of these inputs is systematically varied by incremental steps of 1 μm with a starting position located at 40 μm, 10 μm before the site of the synapse undergoing plastic change and a final position of 60 μm (10 μm past the synapse). One should realise that generally, the STDP window depends on timing differences, the induction site X_{I}, **and** is implicitly influenced by the distance between the induction site and inputs, denoted by X, then the window can be considered to be a function of three variables, X_{I} is the location of STDP induction, and $\mathcal{T} = \Delta T = T_{\mathrm{post}} - t_{\mathrm{pre}}$), denoted as $W(X; X_{\mathrm{I}}, \mathcal{T})$. To characterise the influence

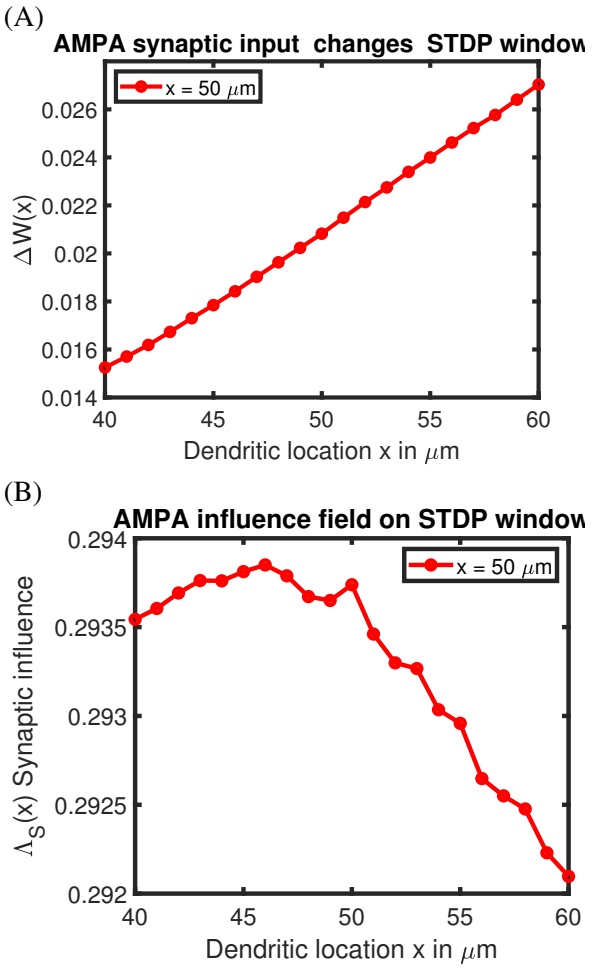

Figure 3: Impact that the additional short train of input spikes has on the STDP induction site at $x = 50\ \mu m$ on the STDP window **(A)** and the corresponding influence field $\rho(x)$ **(B)**. Parameters used for our calcium-based plasticity model were $A = 0.35$, $p_1 = 1$, $p_2 = 1.65$, $p_3 = 3$, $p_4 = 0$, $a_1 = 0.15$, $b_1 = 30$, $a_2 = 0.45$, and $b_2 = 30$.

of short train inputs on the STDP induction site X_I, two measures applied to the resulting STDP windows were adopted. The first and simplest is an L^1 difference measure, denoted by $\Delta W(X)$ between the resulting STDP windows for the case where the short train inputs were present (denoted by $W_{AMPA}(X, X_I, \mathcal{T})$) or absent (denoted by $W_O(X_I, \mathcal{T})$),

$$\Delta W(X) = \int_{\mathcal{T}} \left| W_{AMPA}(X, X_I, \mathcal{T}) - W_O(X_I, \mathcal{T}) \right| d\mathcal{T}.$$

The second measure is an adaptation of the *influence field* originally described in Rathour & Narayanan (2012), given by

$$\Lambda_S(X) = \frac{\left| \omega_O(X_I) - \omega_{AMPA}(X, X_I) \right|}{\omega_O(X_I)},$$

where

$$\omega_O(X_I) = \int_{\mathcal{T}} W_O(X_I, \mathcal{T}) d\mathcal{T}$$

and

$$\omega_{AMPA}(X, X_I) = \int_{\mathcal{T}} W_{AMPA}(X, X_I, \mathcal{T}) d\mathcal{T}.$$

Fig 3 provides an example of the heterosynaptic influence that a short train of inputs has on the resulting STDP window. Here, in **Fig 3A** we can observe that the non-plasticity-inducing inputs lead to clear changes to the STDP window when compared to the case that is absent of these additional inputs. This is due to the activation of calcium-dependent ion channels allowing additional calcium to enter and diffuse in the dendrite and contribute to the expression of the STDP window via calcium-based synaptic plasticity. Note that change in the STDP window profile ($\Delta W(x)$) driven by the short train of inputs increases in size as a function of distance that has a stronger effect at locations posterior to the induction site at $x = 50\ \mu m$, than before. This seeminglessly counter-intuitive observation stems from one's initial expectation that inputs occurring before the induction site would lead to greater changes in the STDP window since these inputs would be expected to contribute more calcium measured at the induction site when compared to inputs occurring after this location. Clearly this is not the case, indicating that inputs occurring after the induction site are contributing more calcium, leading to bigger changes in the resulting STDP window.

The situation is, however, more complicated and strongly dependent on neural excitability, the distribution of ion channels, and in particular, voltage-gated calcium channels, spatial spread of calcium, and any shunting effects originating from the inputs themselves. These are the main factors that contribute to this. The stronger effect from short train inputs occurring after the induction site is likely driven by a combination of spatial diffusion processes for both voltage

and calcium and the input's proximity to a calcium channel hotspot and its proximity to the induction site, leading to more calcium influx when compared to inputs occurring before this site. This suggests that there are non-trivial and likely nonlinear interactions between voltage, calcium influx and diffusion, and calcium (and other) ion channel distributions that have contributed to the observation presented in **Fig 3A**. **Fig 3B**, illustrates the corresponding influence field as a function of distance from the STDP induction site ($x = 50$ μm). Observe the concave profile of $\Lambda_S(x)$ which indicates that the additional inputs occurring after the STDP induction site at $x = 50$ μm has a weaker influence on the resulting STDP window than at locations before $x = 50$ μm.

3.3. Heterosynaptic influence: Impact from altering the number of HVA calcium channel hotspots

In the previous section, we discussed several factors that dictate the observed changes to the STDP window in the presence of additional non-plasticity-inducing inputs. Here, we illustrate that increasing the number of HVA channel hotspots can dramatically alter the L^1 difference measure $\Delta W(x)$ and the influence field $\Lambda_S(x)$. Upon comparing the results from the previous subsection **Fig 4A** shows a similar trend to **Fig 3A**, but influence field $\Lambda_S(x)$ presented in **Fig 4B** has changed from a concave profile (presented in **Fig 3B**) to a near linear relationship similar to the L^1 difference measure (absolute change) in **Fig 4A**. This is a clear example of how changing neural excitability, specifically altering the density of calcium channels can alter the resulting STDP window and the corresponding influence field.

3.4. Heterosynaptic influence depends on spatial location

The heterosynaptic influence field $\Lambda_S(x)$ depends not only on the neural excitability and ion channel hotspot distributions but also on the location of STDP induction along the dendrite. **Fig 5A** and **Fig 5B** demonstrate the changes to the STDP window and the influence field $\Lambda_S(x)$ at a greater distance along the finite cable at $x = 200$ μm, respectively. These profiles are different to those presented in **Fig 3A** and **Fig 3B** for STDP induction at $x = 50$ μm.

Here, the profiles of $\Delta W(x)$ and $\Lambda_S(x)$ align with

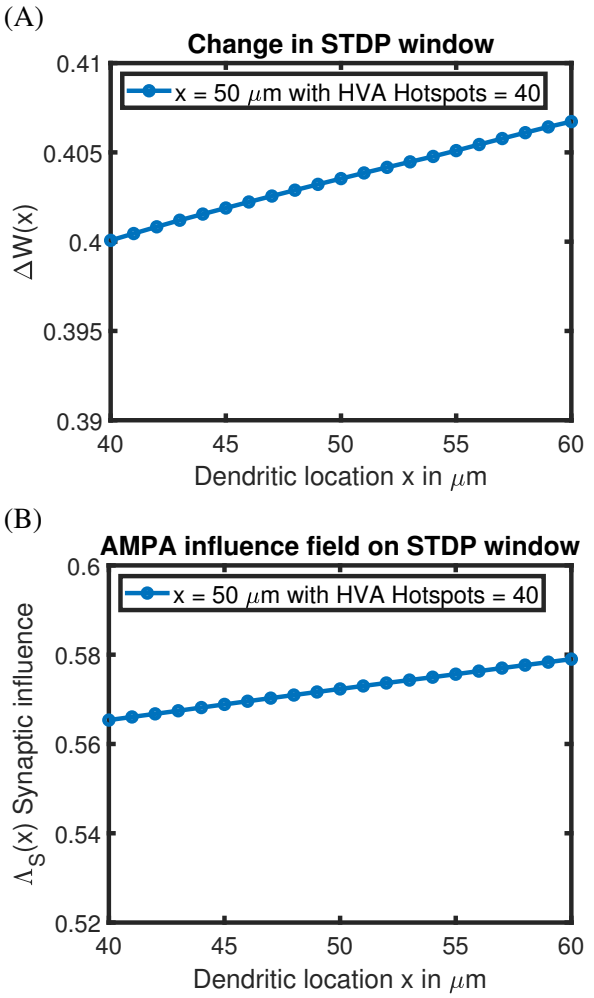

Figure 4: Impact of increasing the number of HVA L-type channel hotspots has on the STDP induction site at $x = 50$ μm. **(A)** is the corresponding L^1 difference measure $\Delta W(x)$ and **(B)** is the corresponding synaptic influence field $\Lambda_S(x)$.

the initial expectation, namely that synaptic inputs occurring before the induction site have a greater influence on the expression of the STDP window than those that occur after this location. One can observe an increase in $\Delta W(x)$ as the position of short train inputs increases, indicating increasing differences between the STDP window and the case when no additional inputs are used, but the influence field at $x = 200$ μm decreases as distance increases suggesting that inputs occurring before the induction site have a stronger influence on the STDP window than inputs occurring afterwards. This stems from inputs occurring before $x = 200$ μm led to a greater influence on the STDP window than those inputs occurring after. This, however, one must not lose sight of the nontrivial interplay between calcium influx

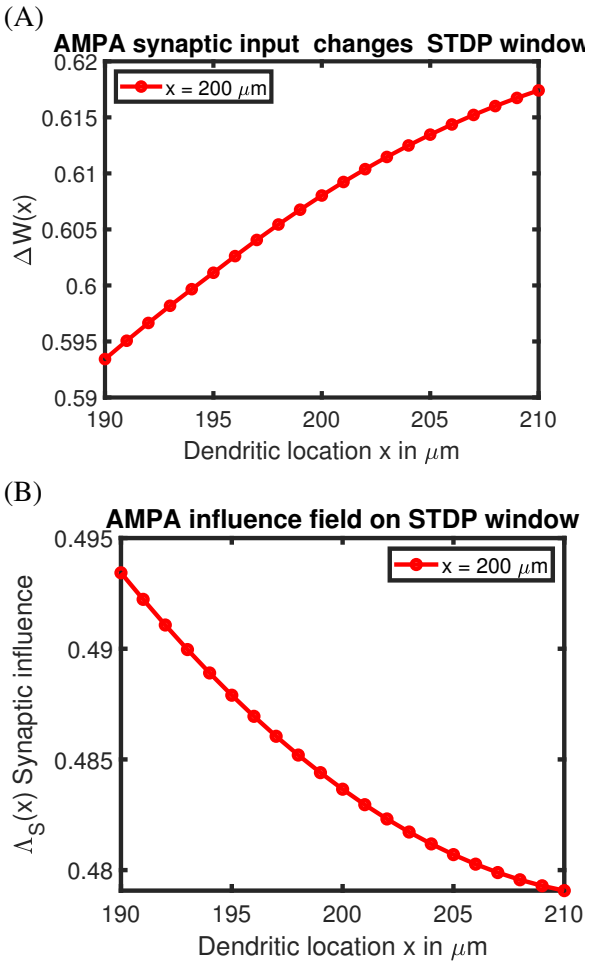

Figure 5: Changing the location of STDP induction to $x = 200\ \mu m$ leads to quantitative changes to **(A)** is the L^1 difference measure $\Delta W(x)$ and **(B)** is the correspinding synaptic influence field $\Lambda_S(x)$.

and diffusion, calcium accumulation, neuronal excitability, the distribution of voltage-activated calcium channels, and the underlying calcium-dependent plasticity rule that generates the STDP window. Furthermore, noting that the functional form of $\Lambda_S(x)$ contains a component that can be interpretted as the relative strength between the STDP window with and without the additional inputs, so as difference between STDP windows increases, this leads to the ratio between the STDP window with and without the additional inputs to increase which leads to a decrease of influence field $\Lambda_S(x)$.

3.5. Heterosynaptic influence also depends on the timing of inputs

In the previous section, the timing of the central input of the train was synchronised with the postsynaptic event. This raises the question of whether the timing onset of these inputs influences has some effect on the resulting STDP window. **Fig 6** presents simulation outcomes that point to a spatiotemporal relationship between the train of inputs, their location relative to the STDP induction site, and their onset timing.

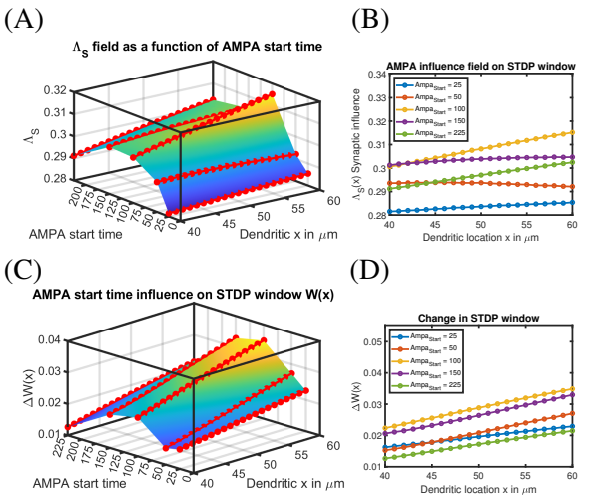

Figure 6: Changing the timing onset of the additional train of inputs relative to the timing of the post-synaptic event at the STDP induction site at $x = 50\ \mu m$ leads to quantitative changes to **(A) and (B)** the influence field $\Lambda_S(x)$ and **(C) and (D)** the L^1 difference measure $\Delta W(x)$

One observes a nonlinear relationship between the timing onset of these inputs, their spatial location relative to the induction site and the corresponding changes to the STDP window. Note that in **Fig 6A** and **Fig 6C** that the interaction field $\Lambda_S(x)$ and L^1 difference measure $\Delta W(s)$ profiles are qualitatively similar, highlighting the presence of nonlocal spatial and temporal heterosynaptic interactions originating from the interplay between the underlying calcium-based plasticity, neuronal excitability, and the distribution of calcium ion channels.

3.6. Inhibitory inputs can influence calcium-derived STDP

The observations presented so far have shown that even a short train of excitatory non-plastic-inducing inputs can influence the expression of plasticity at a different location (with some distance between them), but what about inhibitory inputs? Many studies have often emphasised the importance of inhibitory inputs and their

role in shaping the function of neurons and neural circuits. Driving this is not only the process of plastic change at individual excitatory and inhibitory synapses but also the nature of the spatiotemporal summation of excitatory and inhibitory inputs along neuronal dendrites. Synaptic summation between (excitatory and inhibitory) inputs can be linear or nonlinear, depending on the relative distance and the order between them.

Notably, the summation between an excitatory input followed by an inhibitory input differs from when an inhibitory input is followed by an excitatory one (Tuckwell, 1988*ab*). The synergetic effects of inhibitory inputs are also implicated in dynamically moulding functional dendritic subdomains and plasticity (Gidon & Segev, 2012). This promotes the question of how inhibitory inputs, while in the presence of excitation, impact the resulting STDP window. **Fig 7** highlights a short train of inhibitory inputs had a strong impact on the L^1 distance measure $\Delta W(x)$ and the influence field $\Lambda_S(x)$ when compared to the results presented in **Fig 3**, for the case when inhibitory inputs occur outside of the range of changing location excitatory inputs at on-path and off-path locations **Fig 7A-B** and when inhibition occurs inside this domain of excitation at $x = 45\ \mu m$ and $x = 55\ \mu m$. Here, we see that inhibitory inputs to some degree have equalised the effect of excitatory inputs on STDP and to achieve this the inhibitory inputs seem to be employing a shunting mechanism and further illustrating that off-path inhibition occurring further away from a site of excitatory inputs have a stronger inhibitory effect than on-path inhibition (Gidon & Segev, 2012). One can see a similar effect that off-path inhibition has a strong impact on both $\Delta W(x)$ and the influence field $\Lambda_S(x)$.

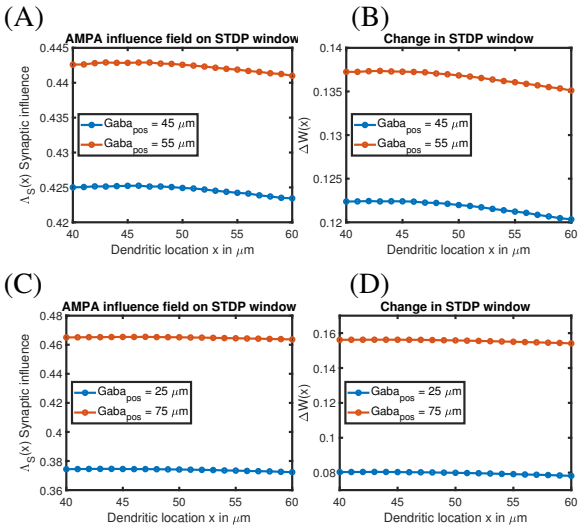

Figure 7: Adding in a short train of inhibitory inputs at four different locations leads to changes to the influence field $\Lambda_S(x)$ and difference measure $\Delta W(x)$ through nonlinear spatial excitatory-inhibitory summation.

4. Discussion

Analytical solutions of cable equations have been sidestepped in past decades with discrete isopotential compartments (D'Angelo & Jirsa, 2022). These compartments result from applying numerical methods that approximate the cable equation by a series of connected isopotential compartments allowing the cable equation to be recast into a system of differential equations, which can be solved numerically. This approach has been extensively used, and the notion of biophysical realism has long been associated with (morphologically detailed) compartmental models (see, e.g., Kobayashi et al. (2021)) or to a lesser extent with reduced compartmental models (see e.g., Elbasiouny (2014)). Yet, compartment models developed by Berman at NIH in the 1960s are susceptible to being mathematically misconstrued (see Lindsay et al. (2007)). Moreover, when the number of compartments approaches infinity the solutions to the discrete and continuous cable equations are expected to converge, however for a finite number of compartments, the discrete version of cable equations does not represent the same dynamics as a continuous cable (see Brzychczy et al. (2012)). This potentially places serious doubt on the validity of compartmental modelling that has been overlooked.

Retro to the common approach in early cable theory was that applied currents represented synaptic inputs, not by conductance changes in series with the driving potential (see Jack et al. (1983)). The driving potential can be considered constant for very small voltage fluctuations in the membrane potential from the resting level, so the conductance change approximates the current waveform. Treating synaptic current as a conductance change in

the cable equation to accurately model synaptic activity, we call it linear cable with reversal "synaptic" potentials (Rall, 1977; Tuckwell, 1985 1988*a*) distributed continuously along the membrane. However, dendritic cable exhibited a sparsity in the distribution of synaptic inputs and ionic channels, and this requires a linear cable with ionic channels.

Ionic cable theory (Poznanski & Bell, 2000*ab*) adequately includes the discreteness of ion-channel density distribution peppered along the dendrites, which includes sparsely distributed ionic channel distribution along the dendritic cable. The cell-level components of such models include the rich repertoire of voltage-dependent ionic channels present in the dendrites of neurons. The rationale is that a continuous distribution of voltage-dependent ion channels, as expressed in cable theory, is an inappropriate approximation for dendrites with channels occurring in low densities. Furthermore, the theory reasonably amplifies the synaptic potentials in neocortical neurons (Stuart & Sakmann, 1995).

The application of *ionic cable theory* to a small-scale neural network level was previously attempted (see Poznanski (2001 2002*ab* 2005)). A significant leap in constructing such biophysically realistic neural network models was identifying and including the cellular components in an analytical description of neural network phenomena. These new models address the relationship between the single neuron's physico-chemical processes (expressed in terms of biophysical mechanisms) with mechanisms at the network level. Such models also consider the rich repertoire of voltage-dependent ionic channels present in the dendrites of neurons but not in a large-scale neural network. This will require extensive use of matrix algebra and Green's function matrices commonly employed in theoretical physics.

Another more realistic approach for the dispersion of spatially extended synaptic spines along the dendritic cable was developed by Basser (1993 2004), who had derived equations for the nodal distribution in the myelinated axons where Heaviside step functions defined the spatial distribution of the nodes where synaptic input reflects upon a small spatial region of a dendritic cable. Dendritic neuron models, as described in Rall et al. (1992), for example, are inadequate for the description of spontaneous activity of neurons in vivo, since the resultant synaptic current input is a random walk of which a smoothed version or a diffusion approximation is Gaussian white noise. Stochastic cable models with white-noise current inputs have been used to mimic random synaptic bombardment in generating spontaneous voltage fluctuations of the membrane potential (Wan & Tuckwell, 1979 1980).

Iannella & Tanaka (2006) extended the "ionic cable theory" to include calcium as a second messenger. The subsequent work by Iannella et al. (2014) considered the role of calcium dynamics in synaptic plasticity. At the same time, we extended this approach to a greater repertoire of channels, which would provide the realism needed to apply the model to explain phenomena like retinal direction selectivity (in preparation). Further work will be needed to extend the modelling to large-scale neuronal networks with a full set of voltage-dependent ionic channels based on "ionic cable theory" using Green's function matrices.

In parallel, many studies have focused on calcium's role in synaptic plasticity and how it shapes synaptic weight of single synapses on the dendrites of neurons using simulations (Castellani et al., 2001; Mäki-Marttunen et al., 2020; Shouval et al., 2002; Yeung et al., 2004; **?**) or experiments (Debanne et al., 1998; Inglebert et al., 2020; Kampa et al., 2006; Tazerart et al., 2020) (For a recent review see (Debanne & Inglebert, 2023)). Consequently, there is increasing interest in the role of calcium across multiple nearby synapses on sections of neurite and associated heterosynaptic plastic events resulting from stimulation, plasticity induction at a dendritic site and how this alters the synaptic weight or the threshold for plastic change in unactivated nearby synapses (Abraham & Goddard, 1983; Chater & Goda, 2021; Chistiakova & Volgushev, 2009; Chistiakova et al., 2014; Harvey & Svoboda, 2007; Kourosh-Arami et al., 2023; Moldwin et al., 2023; Pozo & Goda, 2010). This is, however, one side of the coin of an overarching theme we have called *Heterosynaptic interactions*

due to the bidirectional nature of voltage and calcium signalling in dendrites. This inspired us to look at (what seems to be) the opposing view of how spatial interactions between non-plastic-inducing synaptic inputs influence the intracellular calcium level and the expression of plasticity at the induction site. We have illustrated how spatial summation of inputs to a dendrite segment can affect the resulting expression of an STDP window derived from calcium-dependent plasticity, emphasising that patterns of non-plastic-inducing inputs introduce a distance-dependent spatiotemporal influence. Despite there being many ways to study heterosynaptic influences in dendrites, we decided to use non-plastic-inducing AMPA inputs originating from a short train of eleven spikes, in addition to pre- and post-synaptic input used to calculate the resulting STDP window for the synapse that contains NMDA. The middle spike was synchronised with the back-propagating action potential.

These brief input trains were colocalised and triggered AMPA receptor currents at some fixed distance from the STDP induction site, and were systematically moved in increments of 1 μm steps with respect to the induction site, starting at 10 μm before the induction site and ending at a final position 10 μm past this site. We found detectable changes in the STDP window and quantified them using two different measures ($\Delta W(x)$ and an influence field $\Lambda_S(x)$) indicating a distance-dependent interaction driven by these additional inputs. Notably, this interaction is not fixed and depends on neuronal excitability, ion channel distributions and specifically voltage-activated calcium channels, the location of the induction site on the dendrite, the distance between this site and the inputs, and the onset time of the input train. We showed that the profiles of ΔW and the influence field $\Lambda_S(x)$ as a function of distance from the induction site and time (the difference between the timing of a post-synaptic event and the onset of the input train). We found that the spatiotemporal profiles of these measures, presented in **Fig 6**, were not flat but possessed curvature along the temporal domain. These profiles illustrate a novel nonlinearity associated with location-dependent heterosynaptic interactions and highlights the nontrivial nature of such interactions and their effects on plasticity outcomes when compared to the case when no additional input spike train was used. Underlying such spatiotemporal interactions is a nontrivial interplay between calcium influx, accumulation, and diffusion, neuronal excitability, and the calcium-dependent plasticity rule that generates the resulting STDP window, where the distance between inputs and the site of STDP induction and the nearby calcium channel hotspots to the induction site provide the largest contributions that change the STDP window.

We further investigated where a train of inhibitory inputs was given as an additional stimulation to the dendrite along with the short train of excitatory inputs at specific on-path and off-path locations to the induction site. As shown in **Fig 7**, we observe that inhibition equalises the nonlinear effects caused by the excitatory inputs, since inhibition typically introduces a shunting mechanism resulting in a stronger inhibitory effect for off-path inhibition occurring distal to the induction site than on-path locations. Our results are in agreement with Gidon & Segev (2012) since stronger shunting effects from off-path inhibition results in larger changes to the resulting STDP window $\Delta W(x)$ and a stronger influence field $\Lambda_S(x)$. Heterosynaptic interactions can also play a useful functional role in providing a modulatory error signal back to the synapse undergoing plastic change to modulate calcium accumulation and influence the resulting STDP window. Moreover, such heterosynaptic interactions can also be crucial to excitatory-inhibitory balance (Hiratani & Fukai, 2017). Significantly, our work complements and greatly improves upon the study of Hiratani & Fukai (2017), who considered a simplified compartmental model of a dendritic spine with a phenomenological model of calcium-based plasticity to show how heterosynaptic plasticity can establish excitatory-inhibitory balance; we used a cable-based model for voltage and calcium dynamics and a physiologically-inspired calcium-dependent plasticity model to quantify and map heterosynaptic interactions caused by excitatory and inhibitory inputs along a section of dendrite using the L^1 measure and an interaction field $\Lambda_S(x)$ by illustrating their spatiotemporal characteristics.

Synaptic plasticity (including learning and memory) is a topic that is constantly under intense investigation both experimentally and

theoretically (Abarbanel et al., 2003 2002; Araki et al., 2024; Bliss & Lomo, 1973; Dudek & Bear, 1993; Gerstner et al., 1996; Graupner & Brunel, 2007; Holcman & Schuss, 2005; Holcman & Triller, 2006; Iannella et al., 2010; Kavalali & Monteggia, 2020; Kirkwood et al., 1996; Korkotian et al., 2004; Lee et al., 2024; Magee & Grienberger, 2020; Nishiyama et al., 2000; Pozo & Goda, 2010; Rubin et al., 2005; Shouval et al., 2002; Song & Abbott, 2001; Song et al., 2000) For over 50 years, there have been several modelling methodologies and approaches that have used, ranging from phenomenological models (Graupner & Brunel, 2007; Rubin et al., 2005; Shouval et al., 2002; Song et al., 2000) to those that incorporate calcium diffusion models (Bell & Rangamani, 2023; Earnshaw & Bressloff, 2010; Friedhoff et al., 2021; Holcman & Schuss, 2005; Holcman & Triller, 2006; Korkotian et al., 2004; Mäki-Marttunen et al., 2020).

The majority of studies have relied on point neuron or single compartment models to describe the dynamics of real neurons along with an accompanying plasticity rule typically focusing on showing agreement with available experimental data, for example, illustrating how triplet-based spike timing-dependent plasticity (Pfister & Gerstner, 2006) can reproduce frequency effects observed by Sjöström et al. (2001) or demonstrating that calcium-based plasticity (BCM theory) (Shah et al., 2006) can reproduce the inter-spike interactions observed in experiments (Froemke & Dan, 2002). Given these and other achievements, fewer studies have focused on employing networks of spiking neurons. Classically, network-based simulations that also employed synaptic plasticity typically opted to use artificial neural networks to show the development of orientation and direction selectivity, neuronal receptive fields, and visual maps (Tanaka, 1991; Tanaka & Miyashita, 2009; Wimbauer et al., 1997) and fewer still have used spiking neural networks (Bartsch & van Hemmen, 2001; Iglesias & Villa, 2008; Iglesias et al., 2005; Wenisch et al., 2005). Although these models have been useful for testing hypotheses of how synaptic plasticity or calcium-based learning shapes synaptic weigths and connectivity patterns leading to the emergence of functional properties, the usual single compartment description of spiking neurons is not an accurate representation of real neurons and the applied learning (synaptic plasticity) rule is typically a phenomenological in nature. These studies and modelling approaches all have one major drawback, and that is the absence of dendritic dynamics.

In order to go beyond and address such shortcomings, some studies have combined synaptic plasticity with a single biophysically detailed compartmental model (Gidon & Segev, 2009; Iannella & Launey, 2017; Iannella & Tanaka, 2006; Iannella et al., 2010; Rumsey & Abbott, 2006), thus foregoing the network aspects due to the lack of computational resources. An exception are the network models developed by the *Blue Brain Project* and later the *Human Brain Project* at the École Polytechnique Fédérale de Lausanne (EPFL) that are based on morphologically-detailed compartmental models that require large-scale computing resources to carry out simulations, but as stated previously, since the dynamics of a discretised cable is not an exact match to the dynamics of a continuous cable (Brzychczy et al., 2012) there are potential concerns on the accuracy of compartmental models. In response, we have opted for an alternative approach through the development and application of ionic cable theory and applied calcium-based synaptic plasticity. To date, only a small-scale neural network of ionic cables was previously developed (Poznanski, 2001 2002*ab* 2005)), but this did not include calcium dynamics. Further development will be needed to extend our models to large-scale cable-based networks that includes realistic calcium dynamics and voltage-dependent ion channels and the use of Green's function matrices.

Conflicts of interest:

The authors declare no conflict of interest.

Appendix

We calculate the solution to the linear cable subject to our spike-shaped current clamp $\Phi_0(X,T)$ needs to be is given by:

$$\Phi_0(X,T) = \int_0^T \frac{I_A(0,T-s)}{U_{peak}} G(X,0;s)ds$$

where

$$I_A(0,T) = U_o\Big\{10\sin\Big(\frac{2\pi}{150}T\Big)e^{-\mathcal{A}T/7.5} + 67e^{-2\mathcal{A}T} - 70e^{-4\mathcal{A}T} + 3e^{-\mathcal{A}T/24}\Big\}H(T),$$

where $\mathcal{A} = 15$, the Heaviside step function is denoted by $H(T)$ and the Green's function for the voltage system is $G(X,0;T)$ is given by the solution to the following initial value problem:

$$\frac{\partial G}{\partial T}(X,0;T) = \frac{\partial^2 G}{\partial X^2}(X,0;T) - G(X,0;T), \quad T > 0$$
$$G(X,0;0) = 0.$$

The solution corresponds to the response at position X at time T to a unit impulse at $X = 0$ and $T = 0$. For a finite cable with a killed-end boundary condition $G(0,0;T) = -\delta(T)$ at $X = 0$ and a sealed-end condition $\frac{\partial G}{\partial X}(L,0,T) = 0$ at $X = L$, several representations for the Green's function converges for small T (Tuckwell, 1988*a*) for this case, solving the abovementioned initial value problem for the Green's functions leads to the following expression for $G(X,0;T)$,

$$G(X,0;T) = \frac{e^{-T}}{\sqrt{4\pi T^3}}\sum_{n=0}^{\infty}(-1)^n\Big\{[2(n+1)L - X]\exp\Big(-\frac{[2(n+1)L-X]^2}{4T}\Big) + [2nL + X]\exp\Big(-\frac{[2nL+X]^2}{4T}\Big)\Big\}, \quad T > 0.\ 0 < X < L$$

and the Green's function for unit impulses occurring along the cable $G(X,X_i;T)$ is the solution to the following,

$$\frac{\partial G}{\partial T}(X,X_i;T) = \frac{\partial^2 G}{\partial X^2}(X,X_i;T) - G(X,X_i;T) + \delta(X-X_i)\delta(T), \quad T > 0$$
$$G(X,X_i;0) = 0$$

with the following killed-end boundary condition $G(0,X_i;T) = 0$ at $X = 0$ and sealed-end condition $\frac{\partial G}{\partial X}(L,X_i,T) = 0$ at $X = L$ (where L is the electrotonic length). This is calculated using Laplace transforms and series expansions leading to

$$\mathfrak{G}(X,X_i;T) = \sum_{n=0}^{\infty}(-1)^n\Big\{\exp\Big(-\frac{(X+X_i-2(n+1)L)^2}{4T}\Big) - \exp\Big(-\frac{(X-X_i+2(n+1)L)^2}{4T}\Big) + \exp\Big(-\frac{(X-X_i-2nL)^2}{4T}\Big) - \exp\Big(-\frac{(X+X_i+2nL)^2}{4T}\Big)\Big\},$$

and

$$\mathfrak{H}(X_i,X;T) = \sum_{n=0}^{\infty}(-1)^n\Big\{\exp\Big(-\frac{(X_i+X-2(n+1)L)^2}{4T}\Big) - \exp\Big(-\frac{(X_i-X+2(n+1)L)^2}{4T}\Big) + \exp\Big(-\frac{(X_i-X-2nL)^2}{4T}\Big) - \exp\Big(-\frac{(X_i+X+2nL)^2}{4T}\Big)\Big\},$$

Expanding the first few $n = 0,1,2$ terms gives

$$\mathfrak{G}(X,X_i;T) = \Big\{\exp\Big(-\frac{(X-X_i)^2}{4T}\Big) - \exp\Big(-\frac{(X+X_i)^2}{4T}\Big) + \exp\Big(-\frac{(X+X_i-2L)^2}{4T}\Big) + \exp\Big(-\frac{(X+X_i+2L)^2}{4T}\Big) - \exp\Big(-\frac{(X-X_i-2L)^2}{4T}\Big) + \exp\Big(-\frac{(X-X_i+2L)^2}{4T}\Big) + \exp\Big(-\frac{(X-X_i-4L)^2}{4T}\Big) + \exp\Big(-\frac{(X-X_i+4L)^2}{4T}\Big) - \exp\Big(-\frac{(X+X_i-4L)^2}{4T}\Big)$$

$$+\exp\left(-\frac{(X+X_i+4L)^2}{4T}\right)$$
$$+\exp\left(-\frac{(X+X_i-6L)^2}{4T}\right)$$
$$+\exp\left(-\frac{(X-X_i+6L)^2}{4T}\right)\Bigg\}$$

and

$$\mathfrak{H}(X_i,X;T) =$$
$$\left\{\exp\left(-\frac{(X_i-X)^2}{4T}\right)-\exp\left(-\frac{(_iX+X)^2}{4T}\right)\right.$$
$$+\exp\left(-\frac{(X_i+X-2L)^2}{4T}\right)$$
$$+\exp\left(-\frac{(X_i+X+2L)^2}{4T}\right)$$
$$-\exp\left(-\frac{(X_i-X-2L)^2}{4T}\right)$$
$$+\exp\left(-\frac{(X_i-X+2L)^2}{4T}\right)$$
$$+\exp\left(-\frac{(X_i-X-4L)^2}{4T}\right)$$
$$+\exp\left(-\frac{(X_i-X+4L)^2}{4T}\right)$$
$$-\exp\left(-\frac{(X_i+X-4L)^2}{4T}\right)$$
$$+\exp\left(-\frac{(X_i+X+4L)^2}{4T}\right)$$
$$+\exp\left(-\frac{(X_i+X-6L)^2}{4T}\right)$$
$$+\exp\left(-\frac{(X_i-X+6L)^2}{4T}\right)\Bigg\},$$

where the Green's function for a unit impulse at position X_i along the cable is given by,

$$G(X,X_i;T) =$$
$$\frac{e^{-T}}{\sqrt{4\pi T}}\Big\{\mathfrak{G}(X,X_i;T)H(X_i-X)$$
$$+\mathfrak{H}(X_i,X;T)H(X-X_i)\Big\},$$
$$T>0,\ 0<X,X_i<L.$$

Similarly, the corresponding Green's function for the calcium system can be calculated from

$$\frac{\partial G_{\mathrm{Ca}}}{\partial T}(X_{\mathrm{Ca}},X_{\mathrm{Ca,i}};T_{\mathrm{Ca}}) =$$
$$\frac{\partial^2 G}{\partial X_{\mathrm{Ca}}^2}(X_{\mathrm{Ca}},X_{\mathrm{Ca,i}};T_{\mathrm{Ca}})-G(X_{\mathrm{Ca}},X_{\mathrm{Ca,i}};T_{\mathrm{Ca}})$$
$$+\delta(X_{\mathrm{Ca}}-X_{\mathrm{Ca,i}})\delta(T_{\mathrm{Ca}}),$$
$$G_{\mathrm{Ca}}(X_{\mathrm{Ca}},X_{\mathrm{Ca,i}};0)=0$$
$$T_{\mathrm{Ca}}>0,\ 0\le X_{\mathrm{Ca}},X_{\mathrm{Ca,i}}\le L_{\mathrm{Ca}}.$$

The solution corresponds to the response at position X_{Ca} at time T_{Ca} to a unit impulse at $X_{\mathrm{Ca}} = X_{\mathrm{Ca,i}}$ and $T_{\mathrm{Ca}} = 0$. For a finite cable with sealed-end conditions $\frac{\partial G_{\mathrm{Ca}}}{\partial X_{\mathrm{Ca}}}(0,X_{\mathrm{Ca,i}},T_{\mathrm{Ca}}) = 0$ at $X_{\mathrm{Ca}} = 0$ and $\frac{\partial G_{\mathrm{Ca}}}{\partial X_{\mathrm{Ca}}}(L_{\mathrm{Ca}},X_{\mathrm{Ca,i}},T_{\mathrm{Ca}}) = 0$ at $X_{\mathrm{Ca}} = L_{\mathrm{Ca}}$, the corresponding Green's function is

$$G_{\mathrm{Ca}}(X_{\mathrm{Ca}},X_{\mathrm{Ca,i}};T_{\mathrm{Ca}}) = \sum_{n=-\infty}^{\infty}\Bigg\{$$
$$\exp\left(-\frac{(X_{\mathrm{Ca}}-X_{\mathrm{Ca,i}}-2nL)^2}{4T_{\mathrm{Ca}}}\right)$$
$$+\exp\left(-\frac{(X_{\mathrm{Ca}}+X_{\mathrm{Ca,i}}-2nL)^2}{4T_{\mathrm{Ca}}}\right)\Bigg\},$$
$$T_{\mathrm{Ca}}>0,\ 0\le X_{\mathrm{Ca}},X_{\mathrm{Ca,i}}\le L_{\mathrm{Ca}}.$$

The integral expression for $\Phi_0(X,T)$ can be solved analytically but requires the following integrals to be used,

$$\Gamma(-n-v-1;\frac{X^2}{4T}) = \int_{\frac{X^2}{4T}}^{\infty} z^{-v-2-n}exp(-z)dz,$$
$$I=\int_0^T \zeta^v exp\left(\zeta(\alpha-1)-\frac{X^2}{4\zeta}\right)d\zeta,$$

where Γ is the incomplete Gamma function. The calculation is left as an excerise for the reader, see Iannella & Poznanski (2023) for details of a similar calculation for $\Phi_0(X,T)$.

References

Abarbanel, H. D., Gibb, L., Huerta, R. , Rabinovich, M. I. (2003) Biophysical model of synaptic plasticity dynamics. *Biological Cybernetics* **89**, 214–226.

Abarbanel, H. D., Huerta, R. , Rabinovich, M. (2002) Dynamical model of long-term synaptic plasticity. *Proceedings of the National Academy of Sciences* **99**, 10132–10137.

Abraham, W. , Goddard, G. (1983) Asymmetric relations between homosynaptic long-term potentiation and heterosynaptic long-term depression. *Nature* **305**, 717–719.

Araki, Y., Rajkovich, K. E., Gerber, E. E., Gamache, T. R., Johnson, R. C., Tran, T. H. N., Liu, B., Zhu, Q., Hong, I., Kirkwood, A. et al. (2024) Syngap regulates synaptic plasticity and cognition independently of its catalytic activity. *Science* **383**, eadk1291.

Barrionuevo, G., Schottler, F. , Lynch, G. (1980) The effects of repetitive low frequency stimulation on control and potentiated synaptic responses in the hippocampus. *Life Sciences* **27**, 2385–2391.

Bartsch, A. , van Hemmen, J. L. (2001) Combined hebbian development of geniculocortical and lateral connectivity in a model of primary visual cortex. *Biological Cybernetics* **84**, 41–55.

Basser, P. (1993) Cable equation for a myelinated axon derived from its microstructure. *Medical & Biological Engineering & Computing* **31**, S87–S92.

Basser, P. J. (2004) Scaling laws for myelinated axons derived from an electrotonic core-conductor model. *Journal of Integrative Neuroscience* **3**, 227–244.

Bell, M. K. , Rangamani, P. (2023) Crosstalk between biochemical signalling network architecture and trafficking governs ampar dynamics in synaptic plasticity. *The Journal of Physiology* **601**, 3377–3402.

Bi, G.-Q. , Poo, M.-M. (1998) Synaptic modifications in cultured hippocampal neurons: dependence on spike timing, synaptic strength, and postsynaptic cell type. *Journal of Neuroscience* **18**, 10464–10472.

Bliss, T. , Lomo, T. (1973) Long-lasting potentiation of synaptic transmission in the dentate area of the anaesthetized rabbit following stimulation of the perforant path. *Journal of Physiology* **232**, 331–356.

Brzychczy, S., Leszczyński, H. , Poznanski, R. (2012) Neuronal models in infinite-dimensional spaces and their finite-dimensional projections: Part ii. *Journal of Integrative Neuroscience* **11**, 265–276.

Castellani, G. C., Quinlan, E. M., Cooper, L. N. , Shouval, H. Z. (2001) A biophysical model of bidirectional synaptic plasticity: dependence on ampa and nmda receptors. *Proceedings of the National Academy of Sciences* **98**, 12772–12777.

Chater, T. E. , Goda, Y. (2021) My neighbour hetero—deconstructing the mechanisms underlying heterosynaptic plasticity. *Current Opinion in Neurobiology* **67**, 106–114.

Chistiakova, M. , Volgushev, M. (2009) Heterosynaptic plasticity in the neocortex. *Experimental Brain Research* **199**, 377–390.

Chistiakova, M., Bannon, N. M., Bazhenov, M. , Volgushev, M. (2014) Heterosynaptic plasticity: multiple mechanisms and multiple roles. *The Neuroscientist* **20**, 483–498.

De Schutter, E. , Smolen, P. (1998) Calcium dynamics in large neuronal models. *in* C. Koch , I. Segev, eds, 'Methods in Neuronal modeling: From Ions to Networks'. 2 edn. MIT Press. pp. 211–250.

Debanne, D. , Inglebert, Y. (2023) Spike timing-dependent plasticity and memory. *Current Opinion in Neurobiology* **80**, 102707.

Debanne, D., Gahwiler, B. , Thompson, S. (1994) Asynchronous pre- and postsynaptic activity induces associative long-term depression in area CA1 of the rat hippocampus *in vitro*. *Proceedings of the National Academy of Sciences* **91**, 1148–1152.

Debanne, D., Gähwiler, B. , Thompson, S. (1998) Long-term synaptic plasticity between pairs of individual CA3 pyramidal cells in rat hippocampal slice cultures. *Journal of Physiology* **507**, 237–247.

Debanne, D., Shulz, D. , Fregnac, Y. (1995) Temporal constraints in associative synaptic plasticity in hippocampus and neocortex. *Canadian journal of physiology and pharmacology* **73**, 1295–1311.

Dudek, S. , Bear, M. (1992) Homosynaptic long-term depression in area CA1 of hippocampus and the effects of N-methyl-D-aspartate receptor blockade. *Proceedings of the National Academy of Sciences* **89**, 4363–4367.

Dudek, S. , Bear, M. (1993) Bidirectional long-term modification of synaptic effectiveness in the adult and immature hippocampus. *Journal of Neuroscience* **13**, 2910–2918.

D'Angelo, E. , Jirsa, V. (2022) The quest for multiscale brain modeling. *Trends in Neurosciences* **45**, 777–790.

Earnshaw, B. A. , Bressloff, P. C. (2010) A diffusion-activation model of camkii translocation waves in dendrites. *Journal of computational neuroscience* **28**, 77–89.

Elbasiouny, S. M. (2014) Development of modified cable models to simulate accurate neuronal active behaviors. *Journal of Applied Physiology* **117**, 1243–1261.

Frey, U. , Morris, R. (1997) Synaptic tagging and long-term potentiation. *Nature* **386**, 533–536.

Frey, U. , Morris, R. (1998) Synaptic tagging:implications for late maintenance of hippocampal long-term potentiation. *Trends in Neurosciences* **21**, 181–188.

Friedhoff, V. N., Antunes, G., Falcke, M. , de Souza, F. M. S. (2021) Stochastic reaction-diffusion modeling of calcium dynamics in 3d dendritic spines of purkinje cells. *Biophysical Journal* **120**, 2112–2123.

Froemke, R. , Dan, Y. (2002) Spike-timing dependent synaptic modification induced by natural spike trains. *Nature* **416**, 433–438.

Froemke, R., Poo, M.-M. , Dan, Y. (2005) Spike-timing-dependent synaptic plasticity depends on dendritic location. *Nature* **434**, 221–225.

Fujii, S., Saito, K., Miyakawa, H., Ito, K.-I. , Kato, H. (1991) Reversal of long-term potentiation (depotentiation) induced by tetanus stimulation of the input to CA1 neurons of guinea pig hippocampal slices. *Brain Research* **555**, 112–122.

Gerstner, W., Kempter, R., Leo van Hemmen, J. , Wagner, H. (1996) A neuronal learning rule for sub-millisecond temporal coding. *Nature* **383**, 76–78.

Gidon, A. , Segev, I. (2009) Spike-timing–dependent synaptic plasticity and synaptic democracy in dendrites. *Journal of Neurophysiology* **101**, 3226–3234.

Gidon, A. , Segev, I. (2012) Principles governing the operation of synaptic inhibition in dendrites. *Neuron* **75**, 330–341.

Graupner, M. , Brunel, N. (2007) STDP in a bistable synapse model based on CaMKII and associated signaling pathways. *PLOS Computational Biology* **3**, 2299–2323.

Harvey, C. , Svoboda, K. (2007) Locally dynamic synaptic learning rules in pyramidal neuron dendrites. *Nature* **450**, 1195–1202.

Hiratani, N. , Fukai, T. (2017) Detailed dendritic excitatory/inhibitory balance through heterosynaptic spike-timing-dependent plasticity. *Journal of Neuroscience* **37**, 12106–12122.

Holcman, D. , Schuss, Z. (2005) Modeling calcium dynamics in dendritic spines. *SIAM Journal on Applied Mathematics* **65**, 1006–1026.

Holcman, D. , Triller, A. (2006) Modeling synaptic dynamics driven by receptor lateral diffusion. *Biophysical Journal* **91**, 2405–2415.

Iannella, N. , Launey, T. (2017) Modulating stdp balance impacts the dendritic mosaic. *Frontiers in Computational Neuroscience* **11**, 42.

Iannella, N. , Poznanski, R. R. (2023) Approximate analytical solution of a (v,m,h) reduced system for backpropagating action potentials in sparsely excitable dendrites. *Journal of Multiscale Neuroscience* **2**, 350–171.

Iannella, N. , Tanaka (2006) Analytical solutions for nonlinear cable equations with calcium dynamics. I. Derivations. *Journal of Integrative Neuroscience* **5**, 249–272.

Iannella, N. , Tanaka, S. (2007) Analytical solutions for nonlinear cable equations with calcium dynamics. II. Saltatory transmission in a sparsely excitable cable model. *Journal of Integrative Neuroscience* **6**, 241–277.

Iannella, N. L., Launey, T. , Tanaka, S. (2010) Spike timing-dependent plasticity as the origin of the formation of clustered synaptic efficacy engrams. *Frontiers in Computational Neuroscience* **4**, 21.

Iannella, N., Launey, T., Abbott, D. , Tanaka, S. (2014) A nonlinear cable framework for bidirectional synaptic plasticity. *PLOS One* **9**, e102601.

Iannella, N., Tuckwell, H. , Tanaka, S. (2004) Firing properties of a stochastic PDE model of a rat sensory cortex layer 2/3 pyramidal cell. *Mathematical Biosciences* **188**, 117–132.

Iglesias, J. , Villa, A. E. (2008) Emergence of preferred firing sequences in large spiking neural networks during simulated neuronal development. *International Journal of Neural Systems* **18**, 267–277.

Iglesias, J., Eriksson, J., Grize, F., Tomassini, M. , Villa, A. E. (2005) Dynamics of pruning in simulated large-scale spiking neural networks. *Biosystems* **79**, 11–20.

Inglebert, Y., Aljadeff, J., Brunel, N. , Debanne, D. (2020) Synaptic plasticity rules with physiological calcium levels. *Proceedings of the National Academy of Sciences* **117**, 33639–33648.

Isomura, Y. , Kato, N. (1999) Action potential-induced dendritic calcium dynamics correlated with synaptic plasticity in developing hippocampal pyramidal cells. *Journal of Neurophysiology* **82**, 1993–1999.

Isomura, Y., Fujiwara-Tsukamoto, Y., Imanishi, M., Nambu, A. , Takada, M. (2002) Distance-dependent Ni^{2+}-sensitivity of synaptic plasticity in apical dendrites of hippocampal CA1 pyramidal cells. *Journal of Neurophysiology* **87**, 1169–1174.

Jack, J. J. B., Noble, D. , Tsein, R. (1983) *Electric Current Flow in Excitable Cells*. Clarendon Press, Oxford.

Jahr, C. , Stevens, C. (1990) Voltage dependence of NMDA-activated macroscopic conductances predicted by single-channel kinetics. *Journal of Neuroscience* **10**, 3178–3182.

Kampa, B., Letzkus, J. , Stuart, G. (2006) Requirement of dendritic calcium spikes for induction of spike-timing-dependent synaptic plasticity. *Journal of Physiology* **574.1**, 283–290.

Kavalali, E. T. , Monteggia, L. M. (2020) Targeting homeostatic synaptic plasticity for treatment of mood disorders. *Neuron* **106**, 715–726.

Kelleher, R., Govindarajin, A., Jung, H.-Y., Kang, H. , Tonegawa, S. (2004) Translational control by MAPK signaling in long-term synaptic plasticity and memory. *Cell* **116**, 467–479.

Kirkwood, A., Rioult, M. , Bear, M. (1996) Experience-dependent modification of synaptic plasticity in visual cortex. *Nature* **381**, 526–528.

Kobayashi, T., Kuriyama, R. , Yamazaki, T. (2021) Testing an explicit method for multi-compartment neuron model simulation on a gpu. *Cognitive Computation* **15**, 1–14.

Korkotian, E., Holcman, D. , Segal, M. (2004) Dynamic regulation of spine–dendrite coupling in cultured hippocampal neurons. *European Journal of Neuroscience* **20**, 2649–2663.

Kourosh-Arami, M., Komaki, A., Gholami, M., Marashi, S. H. , Hejazi, S. (2023) Heterosynaptic plasticity-induced modulation of synapses. *The Journal of Physiological Sciences* **73**, 33.

Larkum, M., Kaiser, K. , Sakmann, B. (2001) Dendritic mechanisms underlying the coupling of the dendritic with the axonal action potential initiation zone of adult layer 5 pyramidal neurons. *Journal of Physiology* **533**, 447–466.

Lee, C. T., Bell, M., Bonilla-Quintana, M. , Rangamani, P. (2024) Biophysical modeling of synaptic plasticity. *Annual Review of Biophysics* **53**.

Levy, W. , Steward, O. (1979) Synapses as associative memory elements in the hippocampal formation. *Brain Research* **175**, 233–245.

Lindsay, A., Lindsay, K. , Rosenberg, J. (2007) New concepts in compartmental modelling. *Computing and Visualization in Science* **10**, 79–98.

Magee, J. , Johnston, D. (1997) A synaptically controlled, associative signal for hebbian plasticity in hippocampal neurons. *Science* **275**, 209–212.

Magee, J. C. , Grienberger, C. (2020) Synaptic plasticity forms and functions. *Annual Review of Neuroscience* **43**, 95–117.

Mainen, Z. , Sejnowski, T. (1996) Influence of dendritic structure on firing pattern in model neocortical neurons. *Nature* **382**, 363–366.

Mäki-Marttunen, T., Iannella, N., Edwards, A. G., Einevoll, G. T. , Blackwell, K. T. (2020) A unified computational model for cortical post-synaptic plasticity. *Elife* **9**, e55714.

Malenka, R., Kauer, J., Perkel, D., Mauk, M. D., Kelly, P., Nicoll, R. , Waxham, M. (1989) An essential role for postsynaptic calmodulin and protein kinase activity in long-term potentiation. *Nature* **340**, 554–557.

Malenka, R., Kauer, J., Zucker, R. , Nicoll, R. (1988) Postsynaptic calcium is sufficient for potentiation of hippocampal synaptic transmission. *Science* **242**, 81–84.

Markram, H., Lübke, J., Frotscher, M. , Sakmann, B. (1997) Regulation of synaptic efficacy by coincidence of postsynaptic AP and EPSP. *Science* **275**, 213–215.

Metz, A., Jarsky, T., Martina, M. , Spruston, N. (2005) R-type calcium channels contribute to afterdepolarization and bursting in hippocampal CA1 pyramidal neurons. *Journal of Neuroscience* **25**, 5763–5773.

Moldwin, T., Kalmenson, M. , Segev, I. (2023) Asymmetric voltage attenuation in dendrites can enable hierarchical heterosynaptic plasticity. *ENeuro* **10**.

Mulkey, R., Herron, C. , Malenka, R. (1993) An essential role for protein phosphatases in hippocampal long-term depression. *Science* **261**, 1051–1055.

Nishiyama, M., Hong, K., Mikoshiba, K., Poo, M.-M. , Kato, K. (2000) Calcium stores regulate the polarity and input specificity of synaptic modification. *Nature* **408**, 584–588.

Pfister, J.-P. , Gerstner, W. (2006) Triplets of spikes in a model of spike timing-dependent plasticity. *Journal of Neuroscience* **26**, 9673–9682.

Poznanski, R. (2001) Dendritic spike-like potentials in a neural network. *in* R. Poznanski, ed., 'Biophysical Neural Networks: Foundations of Integrative Neuroscience'. Mary Ann Liebert, NY.. pp. 177–214.

Poznanski, R. (2004) Analytical solutions of the Frankenhaeuser-Huxley equations. I. Minimal model for backpropagation of action potentials in sparsely excitable dendrites. *Journal of Integrative Neuroscience* **3**, 267–299.

Poznanski, R. , Bell, J. (2000*a*) A dendritic cable model for the amplification of synaptic potentials by an ensemble average of persistent sodium channels. *Mathematical Biosciences* **166**, 101–121.

Poznanski, R. , Bell, J. (2000*b*) Theoretical analysis of the amplification of synaptic potentials by small clusters of persistent sodium channels in dendrites. *Mathematical Biosciences* **166**, 123–147.

Poznanski, R. R. (2002*a*) Dendritic integration in a recurrent network. *Journal of Integrative Neuroscience* **1**, 69–99.

Poznanski, R. R. (2002*b*) Towards an integrative theory of cognition. *Journal of Integrative Neuroscience* **1**, 145–156.

Poznanski, R. R. (2005) Dendritic integration in a two-neuron recurrent excitatory network model. *in* 'Modeling in the Neurosciences'. CRC Press. pp. 531–554.

Pozo, K. , Goda, Y. (2010) Unraveling mechanisms of homeostatic synaptic plasticity. *Neuron* **66**, 337–351.

Rall, W. (1964) Theoretical significance of dendritic trees for neuronal input-output relations. *in* R. Riess, ed., 'Neural Theory and Modeling'. Stanford University Press. chapter 4, pp. 73–97.

Rall, W. (1977) Core conductor theory and cable properties of neurons. American Physiological Society. pp. 39–97.

Rall, W., Burke, R., Holmes, W., Jack, J., Redman, S. , Segev, I. (1992) Matching dendritic neuron models to experimental data. *Physiol Reviews* **72**, S159–S186.

Rathour, R. K. , Narayanan, R. (2012) Influence fields: a quantitative framework for representation and analysis of active dendrites. *Journal of Neurophysiology* **107**, 2313–2334.

Reymann, K. , Frey, J. (2007) The late maintenance of hippocampal LTP: Requirements, phases, 'synaptic tagging','late-associativity' and implications. *Neuropharmocology* **52**, 24–40.

Rubin, J., Gerkin, R., Bi, G.-Q. , Chow, C. (2005) Calcium time course as a signal for spike-timing-dependent plasticity. *Journal of Neurophysiology* **93**, 2600–2613.

Rumsey, C. C. , Abbott, L. F. (2006) Synaptic democracy in active dendrites. *Journal of Neurophysiology* **96**, 2307–2318.

Sajikumar, S. , Frey, J. (2004*a*) Late-associativity, synaptic tagging, and the role of dopamine during LTP and LTD. *Neurobiology of Learning and Memory* **82**, 12–25.

Sajikumar, S. , Frey, J. (2004*b*) Resetting of 'synaptic tags' is time—and activity dependent in rat hippocampal CA1 *in vitro*. *Neuroscience* **129**, 503–507.

Sajikumar, S., Navakkode, S. , Frey, J. (2007) Identification of compartment- and process-specific molecules required for "synaptic tagging" during long-term potentiation and long-term depression in hippocampal CA1. *Journal of Neuroscience* **27**, 5068–5080.

Sajikumar, S., Navakkode, S., Sacktor, T. , Frey, J. (2004) Synaptic tagging and cross-tagging: The role of protein kinase mζ in maintaining long-term potentiation but not long-term depression. *Journal of Neuroscience* **25**, 5750–5756.

Shah, N. T., Yeung, L. C., Cooper, L. N., Cai, Y. , Shouval, H. Z. (2006) A biophysical basis for the inter-spike interaction of spike-timing-dependent plasticity. *Biological cybernetics* **95**, 113–121.

Shouval, H., Bear, M. , Cooper, L. (2002) A unified model of NMDA receptor-dependent bidirectional synaptic plasticity. *Proceedings of the National Academy of Sciences* **99**, 10831–10836.

Sjöström, P. , Häusser, M. (2006) A cooperative switch determines the sign of synaptic plasticity in distal dendrites of neocortical neurons. *Neuron* **51**, 227–238.

Sjöström, P. J., Turrigiano, G. G. , Nelson, S. B. (2001) Rate, timing, and cooperativity jointly determine cortical synaptic plasticity. *Neuron* **32**, 1149–1164.

Smolen, P. (2007) A model of late long-term potentiation simulates aspects of memory maintenance. *PLOS One* **2**, e445.

Song, S. , Abbott, L. (2001) Cortical development and remapping through spike timing-dependent plasticity. *Neuron* **32**, 339–350.

Song, S., Miller, K. D. , Abbott, L. F. (2000) Competitive hebbian learning through spike-timing-dependent synaptic plasticity. *Nature Neuroscience* **3**, 919–926.

Staubli, U. , Lynch, G. (1990) Stable depression of potentiated synaptic responses in the hippocampus with 1–5 Hz stimulation. *Brain Research* **513**, 113–118.

Stent, G. (1973) A physiological mechanism for Hebb's postulate of learning. *Proceedings of the National Academy of Sciences* **70**, 997–1001.

Stuart, G. , Sakmann, B. (1995) Amplification of epsps by axosomatic sodium channels in neocortical pyramidal neurons. *Neuron* **15**, 1065–1076.

Tanaka, S. (1991) Theory of ocular dominance column formation: Mathematical basis and computer simulation. *Biological Cybernetics* **64**, 263–272.

Tanaka, S. , Miyashita, M. (2009) Constraint on the number of synaptic inputs to a visual cortical neuron controls receptive field formation. *Neural Computation* **21**, 2554–2580.

Tazerart, S., Mitchell, D. E., Miranda-Rottmann, S. , Araya, R. (2020) A spike-timing-dependent plasticity rule for dendritic spines. *Nature Communications* **11**, 4276.

Tong, R., Chater, T. E., Emptage, N. J. , Goda, Y. (2021) Heterosynaptic cross-talk of pre-and postsynaptic strengths along segments of dendrites. *Cell Reports* **34**.

Tuckwell, H. C. (1985) Some aspects of cable theory with synaptic reversal potentials. *Journal of Theoretical Neurobiology* **4**, 113–127.

Tuckwell, H. C. (1988*a*) *Introduction to Theoretical Neurobiology, vol 1, Linear Cable Theory and Dendritic Structure*. Cambridge University Press, New York.

Tuckwell, H. C. (1988*b*) *Introduction to Theoretical Neurobiology, vol 2, Nonlinear and Stochastic Theories*. Cambridge University Press, New York.

Wan, F. Y. , Tuckwell, H. C. (1979) The response of a spatially distributed neuron to white noise current injection. *Biological Cybernetics* **33**, 39–55.

Wan, F. Y. , Tuckwell, H. C. (1980) The response of a nerve cylinder to spatially distributed white noise inputs. *Journal of Theoretical Biology* **87**, 275–295.

Wenisch, O., Noll, J. , Leo van Hemmen, J. (2005) Spontaneously emerging direction selectivity maps in the visual cortex through STDP. *Biological Cybernetics* **93**, 239–247.

Wimbauer, S., Wenisch, O. G., Miller, K. , van Hemmen, J. L. (1997) Development of spatiotemporal receptive fields of simple cells: I. model formulation. *Biological Cybernetics* **77**, 453–461.

Yeung, L. C., Castellani, G. C. , Shouval, H. Z. (2004) Analysis of the intraspinal calcium dynamics and its implications for the plasticity of spiking neurons. *Physical Review E* **69**, 011907.

Zador, A. , Koch, C. (1994) Linearized models of calcium dynamics: Formal equivalence to the cable equation. *Journal of Neuroscience* **14**, 4705–4715.

Zhang, L., Tao, H., Holt, C., Harris, W. , Poo, M.-M. (1998) A critical window for cooperation and competition among developing retinotectal synapses. *Nature* **395**, 37–44.